A Sampled-Data Form of Incremental Nonlinear Dynamic Inversion for Spacecraft Attitude Control

Acquatella, P.; van Kampen, E.; Chu, Q. P.

DOI
10.2514/6.2022-0761

Publication date
2022

Document Version
Final published version

Published in
AIAA SCITECH 2022 Forum

AIAA SciTech Forum
January 3-7, 2022, San Diego, CA & Virtual
AIAA SCITECH 2022 Forum

10.2514/6.2022-0761

A Sampled-Data Form of Incremental Nonlinear Dynamic Inversion for Spacecraft Attitude Control

Paul Acquatella B. *
DLR, German Aerospace Center, D-82234 Oberpfaffenhofen, Germany

Erik-Jan van Kampen † and Qi Ping Chu ‡
Delft University of Technology, 2629 HS Delft, The Netherlands

This paper presents a sampled–data form of the recently reformulated incremental nonlinear dynamic inversion (INDI) applied for robust spacecraft attitude control. INDI is a combined model– and sensor–based approach mostly applied for attitude control that only requires an accurate control effectiveness model and measurements of the state and some of its derivatives. This results in a reduced dependency on exact knowledge of system dynamics which is known as a major disadvantage of model–based nonlinear dynamic inversion controllers. However, most of the INDI derivations proposed in the literature assume a very high sampling rate of the system and its controller while also not explicitly considering the available sampling time of the digital control computer. Neglecting the sampling time and its effect in the controller derivations can lead to stability and performance issues of the resulting closed–loop nonlinear system. Therefore, our objective is to bridge this gap between continuous–time, highly sampled INDI formulations and their discrete, lowly sampled counterparts in the context of spacecraft attitude control where low sampling rates are common. Our sampled–data reformulation allows explicit consideration of the sampling time via an approximate sampled–data model in normal form widely known in the literature. The resulting sampled–data INDI control is still robust up to a certain sampling time since it remains only sensitive to parametric uncertainties. Simulation experiments for this particular problem demonstrate the bridge considered between INDI formulations which allows for low sampling control rates.

I. Introduction

Future small satellite systems are expected to be more performant not only for fine pointing capabilities in data acquisition but also in terms of high agility for maneuverability, e. g., for high dynamic slewing capability to command the platform for fast and flexible data acquisition [1–9]. This emerging field of '*agile Earth Observation*' motivated the development of a high-agility attitude control system [10] for the the satellite platform BIROS (*Bispectral InfraRed Optical System*) [3] while actuated with a redundant array of three orthogonal *'High-Torque-Wheels' (HTW)* [1, 2]. However, for agile reorientation, a challenge arises from the fact that time-optimal slew maneuvers are, in general, not of the *Euler-axis* rotation [11, 12] type; especially whenever the actuators are constrained independently [13]. The topic of optimal spacecraft rotational maneuvers is quite extensive and has been studied for many decades [13–19]. Some of the agile attitude control solutions have been experimentally validated for imaging satellites in-orbit [20]. However, most of the work reported in literature relies on optimization and some form of path planning and trajectory optimization, which might be difficult to implement on-board and in practice. In this paper, we are motivated to find an agile attitude control solution in closed-loop feedback form. This is challenging because of the many nonlinearities involved in reorientation of small satellites as shown in [10, 20] which calls for a robust nonlinear control approach.

Several nonlinear control methodologies have arisen in the past decades; in part to overcome shortcomings of conventional linear techniques, but also to overcome model or parametric uncertainties that can damage the closed-loop stability and convergence of the system. Among the most popular of these control methodologies are *feedback linearization* (FBL), treated extensively in [21–23] and initially based on early papers of Krener and Brockett in the seventies [24, 25], *adaptive control* [26], and *backstepping* [27, 28]. *Nonlinear dynamic inversion* (NDI), which is how feedback linearization is more commonly known in the aerospace literature [29–33], uses an accurate model of

*Research Scientist, Space System Dynamics Department, Institute of System Dynamics and Control
†Assistant Professor, Control and Simulation Section, Faculty of Aerospace Engineering
‡Associate Professor, Control and Simulation Section, Faculty of Aerospace Engineering

the system to entirely or partly cancel its nonlinearities by means of feedback and exact state transformations. This transforms the nonlinear system dynamics into a linear form over a desired region of interest. For the obtained system, conventional linear control techniques can be applied successfully for achieving desired closed-loop dynamics, hence eliminating the need of linearizing and designing different (linear, robust) controllers for several operational points as in gain-scheduling. The motivations behind the application of NDI for flight control systems originate from difficulties with ensuring stability and performance in between operational points of widely-used gain-scheduled controllers. More advanced methods involving robustness and improvements of the method in NDI-based flight control applications have been considered, among many others, in [29, 32–40]. Although initially intended for flight control, NDI for aerospace applications have also found its way for spacecraft control and re-entry vehicles [41–44]. The main disadvantage for the construction of these NDI control laws is that accurate knowledge of the nonlinear system dynamics is required for an explicit cancellation. For this reason, NDI is considered an *explicit* control method where the desired dynamics of the closed-loop system reside in some explicit model to be followed. Therefore, this explicit aspect of NDI-based control laws is considered to be a disadvantage despite its abilities to linearize and decouple certain classes of nonlinear MIMO systems when full knowledge of the nonlinearities is available. Moreover, this model-based aspect is also strongly influenced by modeling uncertainties. In reality, the model mismatch in the implementation of NDI control laws, together with all sensor aspects, delays and biases, can compromise the performance and stability of the controlled system. Many successful attempts have been carried to identify and reduce these aforementioned flaws of NDI-based control laws with regards to robustness. These attempts are focused in improving the robustness of the overall control architecture by means of applying linear robust control in the outer loop of the system. The works [32, 43] combine NDI with the structured singular value (μ-analysis) and $\mathcal{H}_\infty$ synthesis for reentry flight clearance, and significant benefits were found over conventional NDI. However, not all uncertainties were taken into account or they were covered by lumped uncertainties hence introducing conservatism.

Incremental nonlinear dynamic inversion (INDI) has been proposed as a promising sensor-based approach providing high performance and robust nonlinear control for aerospace vehicles without requiring a detailed model of the controlled plant. The INDI approach reduces its dependency on on-board or baseline models while making use of actuator output and angular acceleration measurement feedback. In contrast to regular NDI, this method is inherently *implicit* in the sense that desired closed-loop dynamics do not reside in some explicit model to be followed but result when the feedback loops are closed [36, 37]. Theoretical development of increments of nonlinear control action date back from the late nineties and started with activities concerning 'implicit dynamic inversion' for inversion-based flight control in the works of P. R. Smith, B. J. Bacon *et al.* [33, 36], where the architectures considered in this paper were firstly described. Other designations for these developments found in the literature are 'modified NDI' and 'simplified NDI', but the designation 'incremental NDI' is considered to describe the methodology and nature of these type of control laws better [34, 45–48]. INDI has been elaborated and applied theoretically in the past decade for advanced flight control applications [33, 34, 36–38, 48] as well as in space applications for spacecraft attitude control [49]. More recently, this technique has been applied also in practice for quadrotors using adaptive control [50, 51], and in real flight tests [52–54], verifying its performance and robustness properties against aerodynamic model uncertainties [34, 55, 56] and disturbance rejection [50, 51, 55, 56].

INDI relies on the assumption that for small time increments and high sampling rates, the nonlinear system dynamics in its incremental form is simply approximated by the (linearized) control effectiveness evaluated at the current state. However, previous theoretical stability and robustness proofs for INDI controllers have many drawbacks and were not mathematically consistent as pointed out in [57, 58]. Most of the previous attempts to prove stability were only based on simplifying assumptions and approximated transfer functions and block diagrams [34, 50, 51]. Recently, the INDI control in the literature has been reformulated for systems with arbitrary relative degree and without recurring to cascaded-control structures, i. e., without using a time–scale separation assumption [57, 58]. This reformulation allowed to extended further the incremental nonlinear control approach for Sliding Mode Control [59]. For these new reformulations and extensions, conditions for stability and robustness analyses have been established and analyzed using Lyapunov-based methods. Another nonlinear control method is *time–delay–control* (TDC) [60–62], more commonly known in the motion control and robotics community and pioneered in the 90's by the works of Hsia, and Youcef-Toumi *et al.* [60]. TDC works by estimating and compensating disturbances and system uncertainties (model and parametric) by utilizing time–delayed signals of some of the system variables. In [62] it has been shown that TDC can be rendered equivalent to a PID–control under some assumptions and some discrete sampling considerations. This motivates the question to study how neglecting the sampling time and its effect in the controller derivations can lead to stability and performance issues of the resulting closed–loop nonlinear system [63, 64].

In this paper, we present three main contributions in the context of nonlinear spacecraft attitude control system

design. 1) We revisit the NDI and the reformulated INDI for the spacecraft attitude control problem and introduce a time–delay explicitly in this incremental reformulation of INDI. 2) We consider the reformulated INDI control for the spacecraft attitude control problem and introduce its sampled–data form based on the model from [64, 65] where the nonlinear dynamics are approximated by a discrete model with piece–wise constant inputs. 3) We bridge the gap between continuous–time, highly sampled (100 – 1000 Hz) INDI formulations and their discrete, lowly sampled counterparts in the context of spacecraft attitude control where low sampling rates are common (1 – 10 Hz). In that sense, our sampled–data reformulation allows explicit consideration of the sampling time via an approximate sampled–data model in normal form widely known in the literature.

The outline of this paper is as follows. A nonlinear model of rigid spacecraft equipped with reaction wheels is presented in Section II. Section III presents incremental nonlinear dynamic inversion in continuous–time form while Section IV presents incremental nonlinear dynamic inversion in sampled–data form, both for the particular problem of spacecraft attitude control. Attitude control numerical simulations are presented in Section V. Conclusions are finally presented in Section VI.

II. Spacecraft Model

In this section we describe the nonlinear rotational dynamics model for spacecraft including a generic set of reaction wheels in arbitrary configuration which are driven by exogenous inputs provided by each wheel's powertrain [10, 20]. In this paper we make use of the Modified Rodrigues Parameters (MRPs) [66–68] as they represent a well defined attitude parameterization for all Eigen-axis rotations in the large domain of $0^\circ \leq \theta < 360^\circ$, where θ is the principle angle rotation around the Euler-axis λ. Typically, Euler angles and quaternions are used to parameterize the attitude kinematics of rigid bodies and most attitude controllers are based on these parameterizations. The preference of using MRPs is motivated to address the problem of agile reorientation while using a minimal set of three rigid body attitude coordinates, thus avoiding redundancy of parameters (quaternions) or singularities (Euler angles). The MRP attitude kinematics parameterization and their potential advantages have been shown to be suitable for attitude stabilization and control applications [66–68].

A. Kinematics

Consider first an array consisting of n reaction wheels. Introducing unit vectors $\mathbf{a}_i \in \mathcal{R}^3$ which give the orientation of the spin-axis of each reaction wheel with respect to the spacecraft coordinate system, these are collected in the configuration or alignment matrix given by

$$\boldsymbol{A} = \begin{bmatrix} \mathbf{a}_1 & \mathbf{a}_2 & \cdots & \mathbf{a}_n \end{bmatrix} \in \mathcal{R}^{3\times n} \tag{1}$$

Then each $\mathbf{a}_i$ can define the $i-$th reaction wheel or 'actuator' frame by taking $\mathbf{a}_i$ as the first axis and making the remaining axes constitute an orthogonal frame. In that sense, the kinematics of the $i-$th reaction wheel with respect to its corresponding actuator frame, in terms of its spin-axis angle Φ_w and angular velocity Ω_w, is simply given by

$$\dot{\Phi}_{w,i} = \Omega_{w,i} \qquad i = 1, \ldots, n \tag{2}$$

Consider now the spacecraft equipped with the n reaction wheels just introduced. The MRP vector $\boldsymbol{\sigma}$ expressed in inertial frame is defined in relation to the Euler-axis λ and to the principle angle rotation θ through [66, 68]

$$\boldsymbol{\sigma} = \lambda \tan\frac{\theta}{4} \tag{3}$$

while its kinematic differential equation in relation with the spacecraft angular velocity $\boldsymbol{\omega} \in \mathcal{R}^3$ (in body fixed frame) in vector form is given by [66, 68] as

$$\dot{\boldsymbol{\sigma}} = \frac{1}{4}\left[(1 - \boldsymbol{\sigma}^\top\boldsymbol{\sigma})\boldsymbol{I}_{3\times 3} + 2\boldsymbol{S}(\boldsymbol{\sigma}) + 2\boldsymbol{\sigma}\boldsymbol{\sigma}^\top\right]\boldsymbol{\omega} = \frac{1}{4}\boldsymbol{B}(\boldsymbol{\sigma})\,\boldsymbol{\omega} \tag{4}$$

where the *skew map* $\boldsymbol{S}(\cdot) : \mathcal{R}^3 \mapsto \mathfrak{so}(3)$ is a linear isomorphism between $\mathcal{R}^3$ and the Lie algebra $\mathfrak{so}(3)$ of 3×3 skew-symmetric matrices and is defined such that $\boldsymbol{S}(\boldsymbol{x})\,\boldsymbol{y} = \boldsymbol{x}\times\boldsymbol{y}$ for any $\boldsymbol{x}, \boldsymbol{y} \in \mathcal{R}^3$, or simply as:

$$\boldsymbol{S}(\boldsymbol{x}) = \begin{bmatrix} 0 & -x_3 & x_2 \\ x_3 & 0 & -x_1 \\ -x_2 & x_1 & 0 \end{bmatrix}, \quad \boldsymbol{x} \in \mathcal{R}^3 \tag{5}$$

Moreover, in this paper we will also be interested in the fact that the time derivative of the MRP kinematic differential equation produces the exact relation [68]

$$\ddot{\boldsymbol{\sigma}} = \frac{1}{4}\left[\, \dot{\boldsymbol{B}}(\boldsymbol{\sigma}) \cdot \boldsymbol{\omega} + \boldsymbol{B}(\boldsymbol{\sigma}) \cdot \dot{\boldsymbol{\omega}} \,\right] = \frac{1}{4}\boldsymbol{C}(\boldsymbol{\sigma}, \boldsymbol{\omega}, \dot{\boldsymbol{\omega}}) \tag{6}$$

where

$$\dot{\boldsymbol{B}}(\boldsymbol{\sigma}) \cdot \boldsymbol{\omega} = \frac{1}{2}\Big[\, 2\boldsymbol{\sigma}^{\top}\boldsymbol{\omega}(1 - \boldsymbol{\sigma}^{\top}\boldsymbol{\sigma})\boldsymbol{\omega} - (1 + \boldsymbol{\sigma}^{\top}\boldsymbol{\sigma})\boldsymbol{\omega}^{\top}\boldsymbol{\omega}\boldsymbol{\sigma} - 4\boldsymbol{\sigma}^{\top}\boldsymbol{\omega}\boldsymbol{S}(\boldsymbol{\omega})\boldsymbol{\sigma} + 4(\boldsymbol{\sigma}^{\top}\boldsymbol{\omega})^{2}\boldsymbol{\sigma} \,\Big]$$

which relates the MRP "acceleration" $\ddot{\boldsymbol{\sigma}}$ to the rigid body's angular velocity $\boldsymbol{\omega}$ and angular acceleration $\dot{\boldsymbol{\omega}}$. This relationship will be key for the attitude control design as it will be shown later on.

B. Dynamics

Following the derivations in Karpenko *et al.* [20], we obtain the rotational dynamics model as follows. First, consider the angular momentum of the spacecraft equipped with the reaction wheel array in question

$$\boldsymbol{H} = \boldsymbol{I}\,\boldsymbol{\omega} + \boldsymbol{h} \tag{7}$$

where, expressed in body-fixed frame, $\boldsymbol{H} \in \mathcal{R}^3$ is the total angular momentum of the system, $\boldsymbol{I} \in \mathcal{R}^{3\times3}$ is the constant inertia matrix of the spacecraft when the reaction wheels are rotating freely, $\boldsymbol{\omega} \in \mathcal{R}^3$ is the spacecraft angular velocity, and $\boldsymbol{h} \in \mathcal{R}^3$ is the total angular momentum vector associated with the reaction wheel array. The angular momentum $\boldsymbol{h}$ can be expressed from individual actuator frames to body-fixed frame as

$$\boldsymbol{h} = \boldsymbol{A}\boldsymbol{h}_w = \boldsymbol{A}\,\boldsymbol{I}_{\boldsymbol{w}}\,\boldsymbol{\Omega}, \tag{8}$$

where $\boldsymbol{I}_{\boldsymbol{w}}$ is a diagonal matrix of reaction wheel spin-axis inertia values and $\boldsymbol{\Omega}$ the inertial angular rate of the reaction wheel array. Defining $\boldsymbol{\Omega}_w$ as the angular rate of the reaction wheel relative to the actuator frame [20], we have

$$\boldsymbol{\Omega} = \boldsymbol{\Omega}_w + \boldsymbol{A}^{\top}\boldsymbol{\omega} \tag{9}$$

where the term $\boldsymbol{A}^{\top}\boldsymbol{\omega}$ is the extra angular velocity of the reaction wheels due to rotation of the spacecraft. Combining Eq. 8 with (9) and left–multiplying by $\boldsymbol{A}^{-1}$ gives the angular momentum associated with the reaction wheels

$$\boldsymbol{h}_w = \boldsymbol{I}_{\boldsymbol{w}}(\boldsymbol{\Omega}_w + \boldsymbol{A}^{\top}\boldsymbol{\omega}) \tag{10}$$

Since the wheel angular momentum rate is related to the internal control torque vector generated by the reaction wheels as

$$\dot{\boldsymbol{h}}_w = \boldsymbol{\tau}_w \tag{11}$$

we can obtain the differential equation

$$\dot{\boldsymbol{\Omega}}_w = \boldsymbol{I}_{\boldsymbol{w}}^{-1}\boldsymbol{\tau}_w - \boldsymbol{A}^{\top}\dot{\boldsymbol{\omega}} \tag{12}$$

that describes the reaction wheel dynamics in terms of reaction wheel torques $\boldsymbol{\tau}_w$; these are considered as the exogenous inputs to the system provided by the wheel's powertrain. Because the angular momentum must be conserved in the absence of external perturbations, applying the transport theorem [14, 20] to Eq. (7), the following relation is obtained

$$\left.\frac{\mathrm{d}\boldsymbol{H}}{\mathrm{d}t}\right|_{\mathcal{I}} = \frac{\mathrm{d}}{\mathrm{d}t}\boldsymbol{H} + \boldsymbol{\omega}^{\mathcal{B}/\mathcal{I}} \times \boldsymbol{H} = \boldsymbol{0} \tag{13}$$

where $\mathcal{I}$ and $\mathcal{B}$ denotes the inertial and body frame, respectively, and we had denoted $\boldsymbol{\omega} \equiv \boldsymbol{\omega}^{\mathcal{B}/\mathcal{I}}$ overall in the paper for notation convenience. Using Eq. (10), Eq. (13) can be further expanded as

$$\boldsymbol{I}\,\dot{\boldsymbol{\omega}} + \boldsymbol{A}\,\boldsymbol{I}_{\boldsymbol{w}}\,\dot{\boldsymbol{\Omega}} + \boldsymbol{\omega} \times (\boldsymbol{I}\,\boldsymbol{\omega} + \boldsymbol{A}\,\boldsymbol{I}_{\boldsymbol{w}}\,\boldsymbol{\Omega}) = \boldsymbol{0} \tag{14}$$

Combining Eqs. (12) and (14), the comprehensive nonlinear model for spacecraft dynamics equipped with reaction wheels [20] is given by

$$\boldsymbol{\Gamma}\begin{bmatrix} \dot{\boldsymbol{\omega}} \\ \dot{\Omega}_{w,1} \\ \vdots \\ \dot{\Omega}_{w,n} \end{bmatrix} = \begin{bmatrix} -\boldsymbol{\omega} \times \left(\boldsymbol{I}\,\boldsymbol{\omega} + \boldsymbol{A}\,\boldsymbol{I}_{\boldsymbol{w}}\,\boldsymbol{\Omega}_w + \boldsymbol{A}\,\boldsymbol{I}_{\boldsymbol{w}}\,\boldsymbol{A}^{\top}\boldsymbol{\omega}\right) \\ \tau_{w,1} \\ \vdots \\ \tau_{w,n} \end{bmatrix} \tag{15}$$

where

$$\boldsymbol{\Gamma} = \begin{bmatrix} \boldsymbol{I} + \boldsymbol{A}\boldsymbol{I}_{\boldsymbol{w}}\boldsymbol{A}^\top & \mathbf{a}_1 I_{w,1} & \cdots & \mathbf{a}_n I_{w,n} \\ I_{w,1}\mathbf{a}_1^\top & I_{w,1} & \cdots & 0 \\ \vdots & \vdots & \ddots & \vdots \\ I_{w,n}\mathbf{a}_n^\top & 0 & \cdots & I_{w,n} \end{bmatrix}$$

is an augmented inertia coupling matrix for the full system and therefore always invertible.

C. Full nonlinear spacecraft model

The augmentation of the nonlinear spacecraft dynamics model together with the MRP kinematics can be rewritten as a full model in the generic form of affine n-dimensional multivariable nonlinear system with m inputs u_i and p outputs y_i as

$$\dot{\boldsymbol{x}} = \boldsymbol{f}(\boldsymbol{x}) + \boldsymbol{g}(\boldsymbol{x})\boldsymbol{u} \tag{16a}$$

$$\boldsymbol{y} = \boldsymbol{h}(\boldsymbol{x}) \tag{16b}$$

where $\boldsymbol{x} \in \mathcal{R}^n$, $\boldsymbol{u} \in \mathcal{R}^m$, and $\boldsymbol{y} \in \mathcal{R}^p$. The functions $\boldsymbol{f}(\boldsymbol{x}) = [\, f_1(\boldsymbol{x}) \quad \cdots \quad f_n(\boldsymbol{x}) \,]^\top$, $\boldsymbol{g}(\boldsymbol{x}) = [\, \boldsymbol{g}_1(\boldsymbol{x})^\top \quad \ldots \quad \boldsymbol{g}_m(\boldsymbol{x})^\top \,]^\top \in \mathcal{R}^{n\times m}$, and $\boldsymbol{h}(\boldsymbol{x}) = [\, h_1(\boldsymbol{x}) \quad \cdots \quad h_p(\boldsymbol{x}) \,]^\top$ are assumed to be smooth vector fields continuously differentiable on $\mathcal{R}^n$. In this paper we consider the output MRP as control variables $\boldsymbol{y} = \boldsymbol{h}(\boldsymbol{x}) = \boldsymbol{\sigma}$ and assume to have three reaction wheels ($n_w = 3$) as actuators, hence $\boldsymbol{u} = \boldsymbol{\tau}_w = [\, \tau_{w,1} \quad \tau_{w,2} \quad \tau_{w,3} \,]^\top$, and $p = m = 3$. In the usual case where $p < m$, meaning that there are more control inputs than control variables, the inversion required for input–output linearization is not direct and some form of control allocation is required. Else, when $p > m$, the system is said to be underactuated and therefore the input–output linearization is underdetermined and possibly not feasible. These two cases are however out of the scope of this paper since $p = m$. Considering the vector $\boldsymbol{x} = [\, \boldsymbol{\sigma}^\top \quad \boldsymbol{\omega}^\top \quad \boldsymbol{\Omega}_w^\top \,]^\top$ with $\boldsymbol{\sigma} = [\, \sigma_1 \quad \sigma_2 \quad \sigma_3 \,]^\top$, $\boldsymbol{\omega} = [\, \omega_x \quad \omega_y \quad \omega_z \,]^\top$, and $\boldsymbol{\Omega}_w = [\, \Omega_{w,1} \quad \Omega_{w,2} \quad \Omega_{w,3} \,]^\top$, the full nonlinear system dynamics in Eqs. (16a)–(16b) results in $n = 9$ and is given by:

$$\boldsymbol{f}(\boldsymbol{x}) = \begin{bmatrix} \frac{1}{4}\boldsymbol{B}(\boldsymbol{\sigma})\,\boldsymbol{\omega} \\ \boldsymbol{\Gamma}^{-1}\begin{bmatrix} -\boldsymbol{\omega} \times \left(\boldsymbol{I}\,\boldsymbol{\omega} + \boldsymbol{A}\,\boldsymbol{I}_{\boldsymbol{w}}\,\boldsymbol{\Omega}_w + \boldsymbol{A}\,\boldsymbol{I}_{\boldsymbol{w}}\,\boldsymbol{A}^\top\boldsymbol{\omega}\right) \\ \mathbf{0}_{3\times 1} \end{bmatrix} \end{bmatrix} \tag{17a}$$

$$\boldsymbol{g}(\boldsymbol{x}) = \begin{bmatrix} \mathbf{0}_{3\times 3} \\ \boldsymbol{\Gamma}^{-1}\begin{bmatrix} \mathbf{0}_{3\times 3} \\ \mathbf{1}_{3\times 3} \end{bmatrix} \end{bmatrix} = \boldsymbol{G} \tag{17b}$$

$$\boldsymbol{h}(\boldsymbol{x}) = \boldsymbol{\sigma} \tag{17c}$$

III. Incremental Nonlinear Dynamic Inversion in Continuous-time Form

In this section we revisit incremental nonlinear dynamic inversion in the context of input–output feedback linearization described in (companion) normal form, and we apply this transformation to the attitude control problem. Moreover, we consider the continuous–time descriptions already widely described in the literature [34, 48, 49, 57, 58].

A. Nonlinear Dynamic Inversion Preliminaries

Finding an explicit relationship between the input u and the output y is generally not straightforward because they are not directly related. Consider again the generic model of affine n-dimensional multivariable nonlinear systems described in Eqs. (16a)–(16b). Collecting all differentiated outputs y_i results in m equations in the form of [57, 69]

$$\boldsymbol{y}^{(\rho)} = \boldsymbol{l}(\boldsymbol{x}) + \boldsymbol{M}(\boldsymbol{x})\boldsymbol{u} \tag{18}$$

where

$$\boldsymbol{y}^{(\boldsymbol{\rho})} = \begin{bmatrix} y_1^{(\rho_1)} \\ y_2^{(\rho_2)} \\ \vdots \\ y_m^{(\rho_m)} \end{bmatrix}, \; \boldsymbol{l}(\boldsymbol{x}) = \begin{bmatrix} \mathcal{L}_f^{\rho_1} h_1(\boldsymbol{x}) \\ \mathcal{L}_f^{\rho_2} h_2(\boldsymbol{x}) \\ \vdots \\ \mathcal{L}_f^{\rho_m} h_m(\boldsymbol{x}) \end{bmatrix},$$

$$\boldsymbol{M}(\boldsymbol{x}) = \begin{bmatrix} \mathcal{L}_{g_1}\mathcal{L}_f^{\rho_1-1} h_1(\boldsymbol{x}) & \mathcal{L}_{g_2}\mathcal{L}_f^{\rho_1-1} h_1(\boldsymbol{x}) & \cdots & \mathcal{L}_{g_m}\mathcal{L}_f^{\rho_1-1} h_1(\boldsymbol{x}) \\ \mathcal{L}_{g_1}\mathcal{L}_f^{\rho_2-1} h_2(\boldsymbol{x}) & \mathcal{L}_{g_2}\mathcal{L}_f^{\rho_2-1} h_2(\boldsymbol{x}) & \cdots & \mathcal{L}_{g_m}\mathcal{L}_f^{\rho_2-1} h_2(\boldsymbol{x}) \\ \vdots & \vdots & & \vdots \\ \mathcal{L}_{g_1}\mathcal{L}_f^{\rho_m-1} h_m(\boldsymbol{x}) & \mathcal{L}_{g_2}\mathcal{L}_f^{\rho_m-1} h_m(\boldsymbol{x}) & \cdots & \mathcal{L}_{g_m}\mathcal{L}_f^{\rho_m-1} h_m(\boldsymbol{x}) \end{bmatrix}$$

and $\mathcal{L}_f^{\rho_j} h_j$, $\mathcal{L}_{g_i}\mathcal{L}_f^{\rho_j-1} h_j$ are the Lie derivatives [21, 70] of the scalar functions h_j with respect to the vector fields $\boldsymbol{f}$ and $\boldsymbol{g}_i$, where $j,\ i = 1, 2, \ldots, m$, respectively. Moreover, the system is said to have a vector of relative degree $\boldsymbol{\rho} = [\ \rho_1 \quad \ldots \quad \rho_p\ ]^\top$ at some point $\bar{\boldsymbol{x}} \in \mathcal{R}^n$ of the state–space when there exists a region of interest $\mathcal{D}_0 \subset \mathcal{R}^n$ around $\bar{\boldsymbol{x}}$ such that for all $\boldsymbol{x} \in \mathcal{D}_0$, $\boldsymbol{M}(\boldsymbol{x})$ is nonsingular (i.e., invertible) and $\mathcal{L}_{g_i}\mathcal{L}_f^k h_j(\boldsymbol{x}) = 0,\ 0 \leq k \leq \rho_j - 1,\ 1 \leq i,\ j \leq m$. In other words, the vector of relative degree represents, for each output $y_i, i = 1, \ldots, p$, the number of output differentiations needed for the input to appear [21, 70]. Moreover, the vector of relative degree of the continuous–time nonlinear system satisfies

$$\rho = \|\boldsymbol{\rho}\|_1 = \sum_{i=1}^{m} \rho_i \leq n \tag{20}$$

where ρ is henceforth called the total relative degree of the system. Furthermore, the system is said to have uniform relative degree when $\rho_1 = \rho_2 = \cdots = \rho_m$. Denoting the m outputs y_j and their derivatives up to the $(\rho_j - 1)$ order as new states $\boldsymbol{\xi} = [\ \boldsymbol{\xi}_1 \quad \ldots \quad \boldsymbol{\xi}_m\ ]^\top$, where $\boldsymbol{\xi}_i = [\ \xi_1^i \quad \ldots \quad \xi_{\rho_i}^i\ ]^\top, i = 1, \ldots, m$, and defined as

$$\begin{array}{ccccc} \xi_1^1 := h_1(\boldsymbol{x}), & \xi_2^1 := \mathcal{L}_f h_1(\boldsymbol{x}), & \cdots, & \xi_{\rho_1}^1 := \mathcal{L}_f^{\rho_1-1} h_1(\boldsymbol{x}), \\ \xi_1^2 := h_2(\boldsymbol{x}), & \xi_2^2 := \mathcal{L}_f h_2(\boldsymbol{x}), & \cdots, & \xi_{\rho_2}^2 := \mathcal{L}_f^{\rho_2-1} h_2(\boldsymbol{x}), \\ \vdots & \vdots & & \vdots \\ \xi_1^m := h_m(\boldsymbol{x}), & \xi_2^m := \mathcal{L}_f h_m(\boldsymbol{x}), & \cdots, & \xi_{\rho_m}^m := \mathcal{L}_f^{\rho_m-1} h_m(\boldsymbol{x}), \end{array} \tag{21}$$

if the total relative degree is equal to the order of the system ($\rho = n$), the ρ–coordinates $\xi_i^j,\ j = 1, 2, \ldots, m;\ i = 1, 2, \ldots, \rho_j$, describe fully the nonlinear behavior of the original system, and moreover, the system is said to be full–state feedback linearizable. Otherwise, whenever the total relative degree is strictly less than the order of the system ($\rho < n$), a part of the system dynamics would become unobservable via input–output linearization using the new set of the ρ–coordinates ξ_i^j, and therefore, these coordinates do not fully describe the original system. In such case, the input–output linearization decomposes the dynamics of the nonlinear system into an external part (input–output), described by the ρ–coordinates, and an internal part (unobservable), described by a new set of $(n - \rho)$–coordinates and therefore called the internal dynamics of the system. The unobservable states, usually denoted as $\boldsymbol{\eta} = [\ \eta_1 \quad \ldots \quad \eta_{n-\rho}\ ]^\top$, are defined via smooth functions $\boldsymbol{\phi}(\boldsymbol{x}) = [\ \phi_1 \quad \ldots \quad \phi_{n-\rho}\ ]^\top$ in the neighborhood $\mathcal{D}_0$ of $\boldsymbol{x}$ as

$$\boldsymbol{\eta} = \boldsymbol{\phi}(\boldsymbol{x}) \tag{22}$$

such that

$$\frac{\partial \phi_i}{\partial \boldsymbol{x}} \boldsymbol{g}_j(x) = 0, \quad \text{for } 1 \leq i \leq n - \rho, \quad \text{for } 1 \leq j \leq m, \quad \forall \boldsymbol{x} \in \mathcal{D}_0 \tag{23}$$

Considering a new coordinate–system $\boldsymbol{z}$ defined as

$$\boldsymbol{z} = \boldsymbol{T}(\boldsymbol{x}) = \begin{bmatrix} \boldsymbol{\psi}(\boldsymbol{x}) \\ \boldsymbol{\phi}(\boldsymbol{x}) \end{bmatrix} = \begin{bmatrix} \boldsymbol{\xi} \\ \boldsymbol{\eta} \end{bmatrix} \tag{24}$$

where $\boldsymbol{T}$ represents a diffeomorphism on the domain $\mathcal{D}_0$, then the original nonlinear system can be transformed into the normal form [21, 22, 57, 70] as

$$\dot{\boldsymbol{\xi}} = \boldsymbol{A}_c\boldsymbol{\xi} + \boldsymbol{B}_c\left[\boldsymbol{l}(\boldsymbol{x}) + \boldsymbol{M}(\boldsymbol{x})\boldsymbol{u}\right]\Big|_{\boldsymbol{x}=\boldsymbol{T}^{-1}(z)} \tag{25a}$$

$$\dot{\boldsymbol{\eta}} = \boldsymbol{f}_c(\boldsymbol{\xi},\boldsymbol{\eta}) = \mathcal{L}_f\boldsymbol{\phi}(\boldsymbol{x})\Big|_{\boldsymbol{x}=\boldsymbol{T}^{-1}(z)} = \frac{\partial\boldsymbol{\phi}(\boldsymbol{x})}{\partial\boldsymbol{x}}\boldsymbol{f}(\boldsymbol{x})\Big|_{\boldsymbol{x}=\boldsymbol{T}^{-1}(z)} \tag{25b}$$

$$\boldsymbol{y} = \boldsymbol{C}_c\boldsymbol{\xi} \tag{25c}$$

where the triplet $(\boldsymbol{A}_c, \boldsymbol{B}_c, \boldsymbol{C}_c)$ is in Brunovsky block canonical form, i. e., $\boldsymbol{A}_c = \text{diag}\{\boldsymbol{A}_o^i\}$, $\boldsymbol{B}_c = \text{diag}\{\boldsymbol{B}_o^i\}$, $\boldsymbol{C}_c = \text{diag}\{\boldsymbol{C}_o^i\}$, $i = 1,\ldots,m$, where $(\boldsymbol{A}_o^i, \boldsymbol{B}_o^i, \boldsymbol{C}_o^i)$ is a canonical form representation of a chain of ρ_i integrators

$$\boldsymbol{A}_o^i := \begin{bmatrix} 0 & 1 & 0 & \cdots & 0 \\ 0 & 0 & 1 & \cdots & 0 \\ \vdots & & \ddots & \ddots & \vdots \\ 0 & & \cdots & 0 & 1 \\ 0 & 0 & & \cdots & 0 \end{bmatrix}, \quad \boldsymbol{B}_o^i := \begin{bmatrix} 0 \\ 0 \\ \vdots \\ 0 \\ 1 \end{bmatrix}, \quad \boldsymbol{C}_o^i := \begin{bmatrix} 1 & 0 & \cdots & 0 \end{bmatrix}, \quad i = 1,\ldots,m \tag{26}$$

The transformation $\boldsymbol{T}$ is required to be a diffeomorphism by the necessity of $\boldsymbol{T}$ being invertible (at least locally in $\mathcal{D}_0$), i.e., $\boldsymbol{T}^{-1}(\boldsymbol{T}(\boldsymbol{x})) = \boldsymbol{x},\ \forall\boldsymbol{x} \in \mathcal{D}_0$, in order to recover the original state vector from the new coordinate $\boldsymbol{z}$, together with the necessity of $\boldsymbol{T}$ and its inverse $\boldsymbol{T}^{-1}$ to be smooth mappings in $\mathcal{R}^n$ guaranteeing that the description of the nonlinear system in the new coordinates is still a smooth one. Since it is generally difficult to find a diffeomorphism defined for all $\boldsymbol{x} \in \mathcal{R}^n$, the requirement of having a diffeomorphism well defined for all $\boldsymbol{x} \in \mathcal{D}_0 \subset \mathcal{R}^n$ makes it a local one. Defining the vector $\boldsymbol{\varphi}(\boldsymbol{x})$ and matrix $\boldsymbol{\vartheta}(\boldsymbol{x})$ as

$$\boldsymbol{\varphi}(\boldsymbol{x}) = -\boldsymbol{M}(\boldsymbol{x})^{-1}\boldsymbol{l}(\boldsymbol{x}) \tag{27a}$$

$$\boldsymbol{\vartheta}(\boldsymbol{x}) = \boldsymbol{M}(\boldsymbol{x})^{-1} \tag{27b}$$

and denoting $\boldsymbol{\nu}$ as a virtual control input, the state feedback control law $\boldsymbol{u}$ defined as

$$\boldsymbol{u} = \boldsymbol{\varphi}(\boldsymbol{x}) + \boldsymbol{\vartheta}(\boldsymbol{x})\boldsymbol{\nu} = \boldsymbol{M}(\boldsymbol{x})^{-1}\left[\boldsymbol{\nu} - \boldsymbol{l}(\boldsymbol{x})\right] \tag{28}$$

cancels all nonlinearities in closed-loop in absence of external disturbances and model uncertainties, resulting in the system

$$\dot{\boldsymbol{\xi}} = \boldsymbol{A}_c\boldsymbol{\xi} + \boldsymbol{B}_c\boldsymbol{\nu} \tag{29a}$$

$$\dot{\boldsymbol{\eta}} = \boldsymbol{f}_c(\boldsymbol{\xi},\boldsymbol{\eta}) \tag{29b}$$

$$\boldsymbol{y} = \boldsymbol{C}_c\boldsymbol{\xi} \tag{29c}$$

which is still described in normal form and decomposed into an external (input–output) part and an internal (unobservable) part. This resulting system is now driven by the virtual control input and entirely described in the newly defined $\boldsymbol{z}$–coordinates $(\boldsymbol{\eta},\boldsymbol{\xi})$. The equation $\dot{\boldsymbol{\eta}} = \boldsymbol{f}_c(\boldsymbol{0},\boldsymbol{\eta})$ defines the zero–dynamics of the system which is defined as the internal dynamics that appear in the system when the input and the initial conditions are chosen such that the output is made or kept identically to zero for all $t \geq 0$. Furthermore, the system is said to be minimum phase if the zero–dynamics have an asymptotically stable equilibrium point in the domain of interest [70]. Referring back to the y_i differentiated outputs in Eq. (18), application of the control input in (28) results in m equations in the form of $y_i^{(\rho_i)} = \nu_i,\ i = \{1,\ldots,m\}$, or, with a slight abuse of notation, more compactly as [57, 69]

$$\boldsymbol{y}^{(\rho)} = \boldsymbol{l}(\boldsymbol{x}) + \boldsymbol{M}(\boldsymbol{x})\boldsymbol{u} = \boldsymbol{\nu} \tag{30}$$

and the sought linear input–output relationship between the new input $\boldsymbol{\nu}$ and the output $\boldsymbol{y}$ is obtained as long as $\boldsymbol{\vartheta} = \boldsymbol{M}(\boldsymbol{x})^{-1}$ is nonsingular. Apart from being linear, an interesting result from this relationship is that it is also decoupled since the input ν_i only affects the differentiated output $y_i^{(\rho_i)}$. From this fact, the input transformation (28) is called a *decoupling control law*, and the linear system (30) results in an *integrator–chain*. The integrator–chain (30)

is sought to be rendered exponentially stable with the proper design of $\boldsymbol{\nu}$, for instance (with a proper choice of k_i, $i = 0, 1, \ldots, \boldsymbol{\rho} - 1$) such as

$$\boldsymbol{\nu} = -k_0 \boldsymbol{y} - k_1 \dot{\boldsymbol{y}} - \cdots - k_{\boldsymbol{\rho}-1} \boldsymbol{y}^{(\boldsymbol{\rho}-1)} \tag{31}$$

From this typical control problem it can be seen that the entire system will have two control loops [34, 46, 47]: the inner linearization loop (28), and the outer control loop provided by the design of $\boldsymbol{\nu}$ (31). This resulting NDI control law depends on accurate knowledge of the model and its parameters, hence it is susceptible to model and parametric uncertainties contained in both $\boldsymbol{l}(\boldsymbol{x})$ and $\boldsymbol{M}(\boldsymbol{x})$.

Now we bring back the discussion into spacecraft attitude control for rigid spacecraft models as described in Eq. (17a), where in this case $n = 9$. Recall the output of the system to be the MRP vector $\boldsymbol{y} = \boldsymbol{h}(\boldsymbol{x}) = \boldsymbol{\sigma} = [\, \sigma_1 \quad \sigma_2 \quad \sigma_3 \,]^\top$, meaning that $p = 3$, and therefore the system has a vector of relative degree $\boldsymbol{\rho} = [\, \rho_1 \quad \rho_2 \quad \rho_3 \,]^\top = [\, 2 \quad 2 \quad 2 \,]^\top$ and total relative degree $\rho = 6$. Since $\rho < n$, the input–output linearization will consist of both an external and an internal part, where the internal part is comprised of three $(n - \rho)$ unobservable states. For the design of an attitude controller as in Eq. (28), first we obtain $\boldsymbol{l}(\boldsymbol{x})$ and $\boldsymbol{M}(\boldsymbol{x})$ as follows. First consider

$$\mathcal{L}_f^1 \boldsymbol{h}(\boldsymbol{x}) = \frac{\partial \boldsymbol{\sigma}}{\partial \boldsymbol{x}} \boldsymbol{f}(\boldsymbol{x}) = \frac{1}{4} \boldsymbol{B}(\boldsymbol{\sigma})\, \boldsymbol{\omega} \tag{32}$$

then $\boldsymbol{l}(\boldsymbol{x})$ is given by

$$\boldsymbol{l}(\boldsymbol{x}) = \mathcal{L}_f^2 \boldsymbol{h}(\boldsymbol{x}) = \nabla[\mathcal{L}_f^1 \boldsymbol{h}(\boldsymbol{x})] \boldsymbol{f}(\boldsymbol{x}) \tag{33}$$

where $\nabla[\mathcal{L}_f^1 \boldsymbol{h}(\boldsymbol{x})]$ represents the Jacobian of the MRP kinematics and is given by

$$\nabla[\mathcal{L}_f^1 \boldsymbol{h}(\boldsymbol{x})] = \frac{\partial [\mathcal{L}_f^1 \boldsymbol{h}(\boldsymbol{x})]}{\partial \boldsymbol{x}} = \frac{1}{4} \frac{\partial \big[\boldsymbol{B}(\boldsymbol{\sigma})\boldsymbol{\omega}\big]}{\partial \boldsymbol{x}} = \underbrace{\left[\, \tfrac{1}{4} \frac{\partial \big[\boldsymbol{B}(\boldsymbol{\sigma})\boldsymbol{\omega}\big]}{\partial \boldsymbol{\sigma}} \quad \tfrac{1}{4}\boldsymbol{B}(\boldsymbol{\sigma}) \quad \boldsymbol{0}_{3\times 3} \,\right]}_{\text{purely kinematic and fully known}} \tag{34}$$

from which it can be easily shown that

$$\frac{1}{4} \frac{\partial \big[\boldsymbol{B}(\boldsymbol{\sigma})\boldsymbol{\omega}\big]}{\partial \boldsymbol{\sigma}} = \frac{1}{2} \begin{bmatrix} \omega_x\sigma_1 + \omega_y\sigma_2 + \omega_z\sigma_3 & \omega_z - \omega_x\sigma_2 + \omega_y\sigma_1 & \omega_z\sigma_1 - \omega_x\sigma_3 - \omega_y \\ \omega_x\sigma_2 - \omega_z - \omega_y\sigma_1 & \omega_x\sigma_1 + \omega_y\sigma_2 + \omega_z\sigma_3 & \omega_x - \omega_y\sigma_3 + \omega_z\sigma_2 \\ \omega_y + \omega_x\sigma_3 - \omega_z\sigma_1 & \omega_y\sigma_3 - \omega_x - \omega_z\sigma_2 & \omega_x\sigma_1 + \omega_y\sigma_2 + \omega_z\sigma_3 \end{bmatrix} \tag{35}$$

Finally, $\boldsymbol{M}(\boldsymbol{x})$ is given as

$$\boldsymbol{M}(\boldsymbol{x}) = \mathcal{L}_g \mathcal{L}_f^1 \boldsymbol{h}(\boldsymbol{x}) = \frac{\partial \big[\mathcal{L}_f^1 \boldsymbol{h}(\boldsymbol{x})\big]}{\partial \boldsymbol{x}} \boldsymbol{g}(\boldsymbol{x}) = \nabla[\mathcal{L}_f^1 \boldsymbol{h}(\boldsymbol{x})] \boldsymbol{G} \tag{36}$$

The attitude control design begins by first considering the new coordinate–system given by the local diffeomorphism (24) where the external states $\boldsymbol{\xi} = [\, \boldsymbol{\xi}_1 \quad \boldsymbol{\xi}_2 \quad \boldsymbol{\xi}_3 \,]^\top$ are given by $\boldsymbol{\xi}_i = [\, \xi_i^1 \quad \xi_i^2 \,]^\top = [\, \sigma_i \quad \dot{\sigma}_i \,]^\top$, $i = 1, 2, 3$, and the choice for the remaining internal states $\boldsymbol{\eta} = \boldsymbol{\phi}(\boldsymbol{x}) = [\, \phi_1 \quad \phi_2 \quad \phi_3 \,]^\top$ are written in compact form as

$$\boldsymbol{\phi}(\boldsymbol{x}) = \boldsymbol{H}_{GG} \, [\, \boldsymbol{\omega} \quad \boldsymbol{\Omega}_w \,]^\top \tag{37}$$

where

$$\boldsymbol{H}_{GG} = \left[\, \boldsymbol{G}_{12}^{-1} \quad \boldsymbol{G}_{13}^{-1} \,\right], \quad \boldsymbol{G}_{12} = -\boldsymbol{A}\boldsymbol{I}^{-1}, \quad \boldsymbol{G}_{13} = -(\boldsymbol{I}\,\boldsymbol{I}_{\boldsymbol{w}})^{-1}(\boldsymbol{I} + \boldsymbol{A}\boldsymbol{I}_{\boldsymbol{w}}\boldsymbol{A}^\top)$$

and furthermore, the choice of $\boldsymbol{H}_{GG}$ has been found such that the following condition

$$\boldsymbol{\phi}(\boldsymbol{0}) = \boldsymbol{0}, \quad \frac{\partial \boldsymbol{\phi}}{\partial \boldsymbol{x}} \boldsymbol{g}(\boldsymbol{x}) = \frac{\partial \boldsymbol{\phi}}{\partial \boldsymbol{x}} \boldsymbol{G} = \boldsymbol{0}, \tag{38}$$

is fulfilled according to the definition of $\boldsymbol{\phi}(\boldsymbol{x})$. Then the original nonlinear system can be transformed into the normal form (25) and the state feedback nonlinear dynamic inversion (NDI) control law $\boldsymbol{u}$ is obtained as in (28)

$$\boldsymbol{u} = \boldsymbol{M}(\boldsymbol{x})^{-1} \, [\boldsymbol{\nu} - \boldsymbol{l}(\boldsymbol{x})] = \Big[\nabla[\mathcal{L}_f^1 \boldsymbol{h}(\boldsymbol{x})] \boldsymbol{G}\Big]^{-1} \Big[\boldsymbol{\nu} - \nabla[\mathcal{L}_f^1 \boldsymbol{h}(\boldsymbol{x})] \boldsymbol{f}(\boldsymbol{x})\Big] \tag{39}$$

while denoting $\boldsymbol{\nu}$ as a virtual control input to be considered later. With this NDI control law, and in absence of external perturbations and model uncertainties, the nonlinearity is cancelled resulting in the nominal closed-loop system as

$$\dot{\boldsymbol{\xi}}_{[6]} = \boldsymbol{A}_{c[6\times6]}\boldsymbol{\xi}_{[6]} + \boldsymbol{B}_{c[6\times3]}\boldsymbol{\nu}_{[3]} \tag{40a}$$

$$\dot{\boldsymbol{\eta}}_{[3]} = \boldsymbol{f}_c(\boldsymbol{\xi}_{[6]}, \boldsymbol{\eta}_{[3]}) \tag{40b}$$

$$\boldsymbol{y}_{[3]} = \boldsymbol{C}_{c[3\times6]}\boldsymbol{\xi}_{[6]} \tag{40c}$$

where the subscript indexes indicate the dimensions of the vectors and matrices, and $\boldsymbol{A}_c$, $\boldsymbol{B}_c$, $\boldsymbol{C}_c$ are in Brunovsky block canonical form as in Eq. (26). Furthermore, the internal dynamics characterized in the $\boldsymbol{x}$-coordinates are given by

$$\boldsymbol{f}_c(\boldsymbol{\xi}, \boldsymbol{\eta})\Big|_{\boldsymbol{x}=\boldsymbol{T}^{-1}(\boldsymbol{z})} = \boldsymbol{G}_{12}^{-1}\dot{\boldsymbol{\omega}} - \boldsymbol{G}_{13}^{-1}\dot{\boldsymbol{\Omega}}_w \tag{41}$$

where the zero–dynamics are be given by $\boldsymbol{f}_c(\boldsymbol{0}, \boldsymbol{\eta}) = \boldsymbol{0}$ which makes the system marginally stable at the origin and around the small neighborhood $\mathcal{D}_0$ in consideration, and therefore the spacecraft attitude control system is non-minimum phase. Zero–dynamics defines the internal dynamics of the system when the input and the initial conditions are chosen such that the output is maintained identically to zero at all times. Therefore, whenever $\boldsymbol{\xi} = \boldsymbol{0}$ (which implies $\boldsymbol{\omega} = \boldsymbol{0}$) we obtain from definition that $\dot{\boldsymbol{\omega}} = \boldsymbol{0}$ and $\dot{\boldsymbol{\Omega}}_w = \boldsymbol{0}$. Note that nothing is said about the corresponding $\boldsymbol{\Omega}_w$ which shall remain constant and therefore responsible to keep the angular momentum fixed inertially. Furthermore, since $\nabla[\mathcal{L}_f^1 \boldsymbol{h}(\boldsymbol{x})]\boldsymbol{G}$ is not singular, the linear input–output relationship between $\ddot{\boldsymbol{\sigma}}$ and $\boldsymbol{\nu}$ is obtained as a double–integrator

$$\ddot{\boldsymbol{\sigma}} = \begin{bmatrix} \ddot{\sigma}_1 \\ \ddot{\sigma}_2 \\ \ddot{\sigma}_3 \end{bmatrix} = \begin{bmatrix} \nu_x \\ \nu_y \\ \nu_z \end{bmatrix} = \boldsymbol{\nu} \tag{42}$$

Normally, the error MRP is obtained with a multiplicative approach (by composition of the relative orientations) but since our control structure involves a path planner which commands an attitude profile in increments, we denote $\boldsymbol{e} = \boldsymbol{\sigma}_e = \boldsymbol{\sigma}_d - \boldsymbol{\sigma}$, which is a valid representation of the MRP error for small incremental rotations [71], and therefore $\dot{\boldsymbol{e}} = \dot{\boldsymbol{\sigma}}_e = \dot{\boldsymbol{\sigma}}_d - \dot{\boldsymbol{\sigma}}$. The double-integrator (42) can be therefore rendered exponentially stable with

$$\boldsymbol{\nu} = \ddot{\boldsymbol{\sigma}}_d + \mathbf{k}_D\dot{\boldsymbol{e}} + \mathbf{k}_P\boldsymbol{e} \tag{43}$$

where $\ddot{\boldsymbol{\sigma}}_d$ is the feedforward reference term for tracking tasks, and $\mathbf{k}_D$ and $\mathbf{k}_P$ being 3×3 constant diagonal matrices whose $i-$th diagonal elements $\mathbf{k}_{D_i}$ and $\mathbf{k}_{P_i}$, respectively, are chosen so that the polynomials $s^2 + \mathbf{k}_{D_i}s + \mathbf{k}_{P_i}$ $i = 1, \ldots, n = 3$,

$$s^2 + \mathbf{k}_{D_i}s + \mathbf{k}_{P_i} \; i = 1, \ldots, n = 3 \tag{44}$$

may become Hurtwiz. This results in the exponentially stable and decoupled error dynamics $\ddot{\boldsymbol{e}} + \mathbf{k}_D\dot{\boldsymbol{e}} + \mathbf{k}_P\boldsymbol{e} = \boldsymbol{0}$

$$\ddot{\boldsymbol{e}} + \mathbf{k}_D\dot{\boldsymbol{e}} + \mathbf{k}_P\boldsymbol{e} = \boldsymbol{0} \tag{45}$$

which implies that $\boldsymbol{e}(t) \to \boldsymbol{0}$ as $t \to \infty$.

B. Incremental Nonlinear Dynamic Inversion

The concept of incremental nonlinear dynamic inversion (INDI) amounts to the application of NDI to a system expressed in an incremental form. This improves the robustness of the closed-loop system as compared with conventional NDI since dependency on the accurate knowledge of the plant dynamics is reduced. Unlike NDI, this control design technique is *implicit* in the sense that desired closed-loop dynamics do not reside in some explicit model to be followed but result when the feedback loops are closed [36, 37]. To begin the discussion, we introduce a sufficiently small time–delay λ and define the following deviation variables

$$\dot{\boldsymbol{x}}_0 := \dot{\boldsymbol{x}}(t-\lambda), \quad \boldsymbol{x}_0 := \boldsymbol{x}(t-\lambda), \quad \boldsymbol{u}_0 := \boldsymbol{u}(t-\lambda) \tag{46}$$

which are λ–time–delayed signals of the current state derivative $\dot{\boldsymbol{x}}(t)$, state $\boldsymbol{x}(t)$, and control $\boldsymbol{u}(t)$, respectively. The *explicit* consideration of the time–delay λ in these deviation variables has not been widely considered in the literature; in reality, an infinitesimal time increment is not practically feasible and because of digital implementation of control

systems, the lowest possible delay admissible by these assumptions is given by the actual sampling rate of the on-board digital computer. For highly sampled applications of INDI (100 – 1000 Hz), an associated (approximate) discrete–time model of the plant provides implicit consideration of the sampling time but most often this is done for the angular rate dynamics with a Taylor series approximation and not for the entire plant (with relative degree > 1). Moreover, we will denote

$$\Delta\dot{\boldsymbol{x}} := \dot{\boldsymbol{x}} - \dot{\boldsymbol{x}}_0, \quad \Delta\boldsymbol{x} := \boldsymbol{x} - \boldsymbol{x}_0, \quad \Delta\boldsymbol{u} := \boldsymbol{u} - \boldsymbol{u}_0 \tag{47}$$

as the incremental state derivative, the incremental state, and the so–called incremental control input, respectively. To obtain an incremental form of system dynamics [33, 34, 36–38, 48, 49, 72], we consider the first–order Taylor series expansion of $\boldsymbol{y}^{(\rho)}$ as in [57, 58], not in the geometric sense, but with respect to the newly introduced $\Delta\boldsymbol{x}$ and $\Delta\boldsymbol{u}$ (functions of the time–delay λ) as

$$\boldsymbol{y}^{(\rho)} = \boldsymbol{y}_0^{(\rho)} + \frac{\partial}{\partial \boldsymbol{x}}\Big[\boldsymbol{l}(\boldsymbol{x}) + \boldsymbol{M}(\boldsymbol{x})\boldsymbol{u}\Big]\Big|_{\substack{\boldsymbol{x}=\boldsymbol{x}_0 \\ \boldsymbol{u}=\boldsymbol{u}_0}} \Delta\boldsymbol{x} + \boldsymbol{M}(\boldsymbol{x}_0)\Delta\boldsymbol{u} + O(\Delta\boldsymbol{x}^2) = \boldsymbol{y}_0^{(\rho)} + \boldsymbol{M}(\boldsymbol{x}_0)\Delta\boldsymbol{u} + \boldsymbol{N}(\boldsymbol{x},\lambda) \tag{48}$$

with

$$\boldsymbol{y}_0^{(\rho)} = \boldsymbol{l}(\boldsymbol{x}_0) + \boldsymbol{M}(\boldsymbol{x}_0)\boldsymbol{u}_0 \tag{49a}$$

$$\boldsymbol{N}(\boldsymbol{x},\lambda) = \frac{\partial}{\partial \boldsymbol{x}}\Big[\boldsymbol{l}(\boldsymbol{x}) + \boldsymbol{M}(\boldsymbol{x})\boldsymbol{u}\Big]\Big|_{\substack{\boldsymbol{x}=\boldsymbol{x}_0 \\ \boldsymbol{u}=\boldsymbol{u}_0}} \Delta\boldsymbol{x} + O(\Delta\boldsymbol{x}^2) \tag{49b}$$

and the perturbation term $\boldsymbol{N}(\boldsymbol{x},\lambda)$ as in [57, 58] satisfies

$$\lim_{\lambda\to 0} \|\boldsymbol{N}(\boldsymbol{x},\lambda)\|_2 \to 0, \ \forall\, \boldsymbol{x} \tag{50}$$

This assumption of having high sampling rates such that (50) holds has been widely considered as valid in the incremental nonlinear dynamic inversion and incremental backstepping control literature [52, 54, 72, 73]. From now on, we shall refer to $\boldsymbol{M}(\boldsymbol{x}_0)$ as the *instantaneous control effectiveness (ICE)* matrix, meaning that this model–based term is sampled at each incremental instant. This leaves us with an approximate linearization about the $\lambda-$delayed signals that is performed *incrementally*, and not with respect to a particular equilibrium or operational point of interest. We now introduce a formal assumption to continue with the incremental nonlinear control design.

Time-scale separation (TSS) assumption: *For a sufficiently small time-delay λ and for any (bounded) incremental control input, it is assumed that $\Delta\boldsymbol{x}$ does not vary significantly during λ. In other words, the input rate of change is much faster than the state rate of change, so this is seen as a time-scale separation assumption:*

$$\epsilon_{TSS}(t) \equiv \|\Delta\boldsymbol{x}\|_2 \cong 0, \ \forall\, \Delta\boldsymbol{u} \tag{51}$$

which leads to

$$\|\boldsymbol{N}(\boldsymbol{x},\lambda)\|_2 \cong 0 \tag{52}$$

and therefore

$$\boldsymbol{y}^{(\rho)} \cong \boldsymbol{y}_0^{(\rho)} + \boldsymbol{M}(\boldsymbol{x}_0)\,(\boldsymbol{u} - \boldsymbol{u}_0) \tag{53}$$

This assumption shows that for small time increments (high sampling rates) the nonlinear system dynamics in its incremental form (in relative coordinates) are simply approximated by its instantaneous control effectiveness (ICE) matrix $\boldsymbol{M}(\boldsymbol{x}_0)$, i.e., the control effectiveness evaluated at the current state. Since this results in a change of coordinates (absolute to relative), the development of control laws in the original set of (absolute) coordinates implies or requires the availability of $\boldsymbol{y}_0^{(\rho)}$ and $\boldsymbol{u}_0$ in (53). For the obtained approximation (53), NDI is applied to obtain a relation between the incremental control input and the output of the system

$$\boldsymbol{u} = \boldsymbol{u}_0 + \boldsymbol{M}(\boldsymbol{x}_0)^{-1}[\boldsymbol{\nu} - \boldsymbol{y}_0^{(\rho)}] \tag{54}$$

Note that the incremental input $\boldsymbol{u}_0$ that corresponds to $\boldsymbol{y}_0^{(\rho)}$ is measured or estimated from the output of the actuators, and it has been assumed that a commanded control is achieved sufficiently fast as to being able to neglect the effect of the actuator dynamics. The total control command along with the obtained linearizing control $\boldsymbol{u}_0 = \boldsymbol{u}(t-\lambda)$ can be rewritten as

$$\boldsymbol{u}(t) = \boldsymbol{u}(t-\lambda) + \boldsymbol{M}(\boldsymbol{x}(t-\lambda))^{-1}\left[\boldsymbol{\nu} - \boldsymbol{y}^{(\rho)}(t-\lambda)\right] \tag{55}$$

and its referred to as the incremental nonlinear dynamic inversion (*INDI*) control law. The dependency of the closed–loop system on accurate knowledge of the dynamic model in $\boldsymbol{l}(\boldsymbol{x})$ is largely decreased, improving robustness against model uncertainties contained therein. Therefore, this implicit control law design is more dependent on accurate measurements or accurate estimates of $\boldsymbol{y}_0^{(\rho)}$, the state derivatives, and $\boldsymbol{u}_0$, the incremental control input, respectively. The cancelling of all nonlinearities in closed–loop, in absence of external disturbances and model uncertainties, results in the system

$$\dot{\boldsymbol{\xi}} = \boldsymbol{A}_c\boldsymbol{\xi} + \boldsymbol{B}_c\left[\boldsymbol{\nu} + \boldsymbol{N}(\boldsymbol{x},\boldsymbol{u},\lambda)\right] \tag{56a}$$

$$\dot{\boldsymbol{\eta}} = \boldsymbol{f}_c(\boldsymbol{\xi},\boldsymbol{\eta}) \tag{56b}$$

$$\boldsymbol{y} = \boldsymbol{C}_c\boldsymbol{\xi} \tag{56c}$$

which is still described in normal form. The stability and robustness properties of this system has been thoroughly studied in [57, 58] and the reader is referred to these references for more details. Referring back to the attitude control problem, since we will consider the dynamics in its incremental form as in (48) for the control design, the application of *INDI* results in a control law that is only subject to sensor uncertainties and model uncertainties contained within the estimated ICE matrix $\bar{\boldsymbol{M}}$ as

$$\boldsymbol{u}(t) = \boldsymbol{u}(t-\lambda) + \bar{\boldsymbol{M}}(\boldsymbol{x}(t-\lambda))^{-1}\left[\boldsymbol{\nu} - \boldsymbol{y}^{(\rho)}(t-\lambda)\right] \tag{57}$$

However, notice that

$$\bar{\boldsymbol{M}}(\boldsymbol{x}(t-\lambda)) = \mathcal{L}_g\mathcal{L}_f^1\boldsymbol{h}(\boldsymbol{x}(t-\lambda)) = \frac{\partial\left[\mathcal{L}_f^1\boldsymbol{h}(\boldsymbol{x}(t-\lambda))\right]}{\partial\boldsymbol{x}}\bar{\boldsymbol{g}}(\boldsymbol{x}(t-\lambda)) \tag{58}$$

$$= \underbrace{\nabla[\mathcal{L}_f^1\boldsymbol{h}(\boldsymbol{x}(t-\lambda))]}_{\text{purely kinematic}}\underbrace{\bar{\boldsymbol{G}}}_{\text{purely parametric}} \tag{59}$$

where the only (parametric) uncertainties are contained in the estimated $\bar{\boldsymbol{g}}(\boldsymbol{x}(t-\lambda)) = \bar{\boldsymbol{G}}$ which contains information only about the spacecraft inertia matrix and the inertias of the wheel–set. This means that in the particular case of this plant, namely a rigid body spacecraft actuated with a non-redundant set of orthogonal reaction wheels and parameterized by MRPs, the incremental nonlinear dynamic inversion is robust against uncertainties since the term $\nabla[\mathcal{L}_f^1\boldsymbol{h}(\boldsymbol{x}(t-\lambda))]$, contained in $\boldsymbol{M}(\boldsymbol{x}(t-\lambda))$ is given by a kinematic and known relationship, therefore void of uncertainty. Moreover, this purely kinematic term in the resulting control law is only subjected to the measured errors contained in $\boldsymbol{x}(t-\lambda)$. To conclude the INDI attitude control design, we have made use of the fact that

$$\boldsymbol{y}_0^{(\rho)} = \ddot{\boldsymbol{\sigma}}_0 = \frac{1}{4}\left[\,\dot{\boldsymbol{B}}(\boldsymbol{\sigma}_0)\cdot\boldsymbol{\omega}_0 + \boldsymbol{B}(\boldsymbol{\sigma}_0)\cdot\dot{\boldsymbol{\omega}}_0\,\right] \tag{60}$$

where the relationship

$$\dot{\boldsymbol{B}}(\boldsymbol{\sigma}_0)\cdot\boldsymbol{\omega}_0 = \frac{1}{2}\left[\,2\boldsymbol{\sigma}_0^\top\boldsymbol{\omega}_0(1-\boldsymbol{\sigma}_0^\top\boldsymbol{\sigma}_0)\boldsymbol{\omega}_0 - (1+\boldsymbol{\sigma}_0^\top\boldsymbol{\sigma}_0)\boldsymbol{\omega}_0^\top\boldsymbol{\omega}_0\boldsymbol{\sigma}_0 - 4\boldsymbol{\sigma}_0^\top\boldsymbol{\omega}_0\boldsymbol{S}\left(\boldsymbol{\omega}_0\right)\boldsymbol{\sigma}_0 + 4(\boldsymbol{\sigma}_0^\top\boldsymbol{\omega}_0)^2\boldsymbol{\sigma}_0\,\right] \tag{61}$$

is given and therefore highly beneficial to compute $\ddot{\boldsymbol{\sigma}}_0$ analytically which is otherwise very hard to estimate with finite differences or by approximation since this would amplify the noise contained in measurements. By using the measured $\boldsymbol{y}_0^{(\rho)}$ and commanded $\boldsymbol{u}_0$ incrementally, we practically obtain a nonlinear 'self-scheduling' *NDI* control law that is robust to model and parametric uncertainties. Notice, however, that this *INDI* control law is depending on the instantaneous control effectiveness (ICE) matrix reflected in $\boldsymbol{M}(\boldsymbol{x}_0)$, which in turn is only susceptible to parametric uncertainties in $\boldsymbol{G}$ that are related to inertia values of the rigid body and its reaction wheels. This remark gives a hint to one of the key differences with respect to *time-delay control* (*TDC*), where the control effectiveness is considered as a fixed–gain matrix instead [74].

IV. Incremental Nonlinear Dynamic Inversion in Sampled-Data Form

In this section we are interested in bridging the continuous–time derivation of INDI with respect to a discrete or sampled–time counterpart. In contrast to linear systems where exact sampled-data models can be obtained, for nonlinear systems a sampled–data model can only *approximate* the real dynamics up to a certain degree [63–65]. However, the accuracy of such models can be characterised in a precise way. Considering an analogous system to (16) but described as a sampled–data model, we will derive parallels in terms of incremental control design but recalling that these models are obtained as an approximation of the input–output mapping of the nonlinear forms already system presented.

A. Preliminaries

Since a sampled–data model is sought such that it closely approximates the nonlinear input–output mapping given in the previous section, we may obtain these approximations by considering that the control inputs $\boldsymbol{u}(t)$ are provided in sampled–time by a *zero–order hold* (ZOH). When assuming the input comes from a digital–to–analog converter as such zero–order hold signals, the input is hence generated as piece–wise constant signals. Such piece–wise constant inputs are provided in between sampling time intervals of amplitude λ are given by

$$\boldsymbol{u}(t) := \boldsymbol{u}_k = \boldsymbol{u}(k\lambda), \quad \text{for} \quad t \in [k\lambda, (k+1)\lambda), \quad k \geq 0 \tag{62}$$

where $k \in \mathcal{Z}^+$ is the sampled or discrete–time index [64]. Furthermore, recalling the shift–operator q that shifts the current state as $q\boldsymbol{x}_k = \boldsymbol{x}_{k+1}$, we will be interested in using the δ–operator [64, 65] defined as

$$\delta = \frac{q-1}{\lambda} \tag{63}$$

which corresponds to a reparameterisation of sampled–data models that allows to explicitly include the sampling period in a discrete–time description [75]. Denoting $\boldsymbol{x}_k = [\, x_{k_1} \quad \cdots \quad x_{k_n} \,]^\top \in \mathcal{R}^n$ as the sampled–time state sequence, $\boldsymbol{y}_k = [\, y_{k_1} \quad \cdots \quad y_{k_p} \,]^\top \in \mathcal{R}^p$ as the sampled–time output sequence, and $\boldsymbol{u}_k = [\, u_{k_1} \quad \cdots \quad u_{k_m} \,]^\top \in \mathcal{R}^m$ as the piece–wise continuous and sampled–time input sequence, an approximated sampled–data (discrete–time) dynamics model corresponding to (16) will result in a model of the form

$$\delta\boldsymbol{x}_k = \boldsymbol{f}_k(\boldsymbol{x}_k) + \boldsymbol{g}_k(\boldsymbol{x}_k)\boldsymbol{u}_k \tag{64a}$$

$$\boldsymbol{y}_k = \boldsymbol{h}_k(\boldsymbol{x}_k) \tag{64b}$$

where the functions $\boldsymbol{f}_k(\boldsymbol{x}_k) = [\, f_{k_1}(\boldsymbol{x}_k) \quad \cdots \quad f_{k_n}(\boldsymbol{x}_k) \,]^\top$, $\boldsymbol{g}_k(\boldsymbol{x}_k) = [\, \boldsymbol{g}_{k_1}(\boldsymbol{x}_k)^\top \quad \ldots \quad \boldsymbol{g}_{k_m}(\boldsymbol{x})^\top \,]^\top \in \mathcal{R}^{n\times m}$, and $\boldsymbol{h}_k(\boldsymbol{x}_k) = [\, h_{k_1}(\boldsymbol{x}_k) \quad \cdots \quad h_{k_p}(\boldsymbol{x}) \,]^\top$ are assumed to be analytical approximations of the original nonlinear model, and therefore smooth vector fields continuously differentiable on $\mathcal{R}^n$.

B. A Sampled–Data Model for Deterministic Nonlinear Systems

Yuz and Goodwin [64, 65] presented a sampled–data model as in Eqs. (64a)-(64b) for deterministic nonlinear systems. The model results in a truncation error of order $[\, \lambda^{\rho_1+1} \quad \ldots \quad \lambda^{\rho_p+1} \,]^\top$ between the sampled–data model output $\boldsymbol{y}_k$ and the continuous–time output $\boldsymbol{y}(t)$ of the original system (16a)–(16b) at sampling instants $t = k\lambda$ when the inputs $\boldsymbol{u}(t)$ are generated from $\boldsymbol{u}_k$ as sampled–time and piece–wise constant (ZOH) control inputs. The fact that this model is close in a well defined sense to the continuous–time output helps to bridge the connection between continuous–time incremental nonlinear control methods and their discrete or sampled–time counterparts in appropriate fashion. Moreover, the key fact of using models described as in (64) is that these are models already given in *incremental form*, but in the discrete sense, i.e., as state transitions represented as

$$\boldsymbol{x}_{k+1} = \boldsymbol{x}_k + \lambda \cdot \delta\boldsymbol{x}_k \tag{65}$$

where also the sampling time λ is considered *explicitly*. Denoting $\boldsymbol{\xi}_k = [\, z_{k_1} \quad \cdots \quad z_{k_\rho} \,]^\top$ and $\boldsymbol{\eta}_k = [\, z_{k_{\rho+1}} \quad \cdots \quad z_{k_n} \,]^\top$, we can consider the new coordinate–system defined as

$$\boldsymbol{z}_k = \boldsymbol{T}_s(\boldsymbol{x}_k) = \begin{bmatrix} \boldsymbol{\psi}_s(\boldsymbol{x}_k) \\ \boldsymbol{\phi}_s(\boldsymbol{x}_k) \end{bmatrix} = \begin{bmatrix} \boldsymbol{\xi}_k \\ \boldsymbol{\eta}_k \end{bmatrix} \tag{66}$$

where clearly $\boldsymbol{z}_k = [\, z_{k_1} \quad \cdots \quad z_{k_n} \,]^\top$ and $\boldsymbol{T}_s$ defines the diffeomorphism on the domain $\mathcal{D}_0$, and then the original continuous-time nonlinear system (16a)–(16b) system can be approximated as the following discrete normal form [64, 65]

$$\delta\boldsymbol{\xi}_k = \boldsymbol{A}_s\boldsymbol{\xi}_k + \boldsymbol{B}_s\left[\boldsymbol{l}(\boldsymbol{\xi}_k,\boldsymbol{\eta}_k) + \boldsymbol{M}(\boldsymbol{\xi}_k,\boldsymbol{\eta}_k)\boldsymbol{u}_k\right] \tag{67a}$$

$$\delta\boldsymbol{\eta}_k = \boldsymbol{f}_s(\boldsymbol{\xi}_k,\boldsymbol{\eta}_k) \tag{67b}$$

$$\boldsymbol{y}_k = \boldsymbol{C}_s\boldsymbol{\xi}_k \tag{67c}$$

where the triplet $(\boldsymbol{A}_s, \boldsymbol{B}_s, \boldsymbol{C}_s)$ is in Brunovsky block canonical form, i. e., $\boldsymbol{A}_s = \text{diag}\{\boldsymbol{A}_k^i\}$, $\boldsymbol{B}_s = \text{diag}\{\boldsymbol{B}_k^i\}$, $\boldsymbol{C}_s = \text{diag}\{\boldsymbol{C}_k^i\}$, $i = 1, \ldots, m$, and $(\boldsymbol{A}_k^i, \boldsymbol{B}_k^i, \boldsymbol{C}_k^i)$ are given as the following matrices [64, 65]

$$\boldsymbol{A}_k^i := \begin{bmatrix} 0 & 1 & \lambda/2 & \cdots & \frac{\lambda^{\rho_i-2}}{(\rho_i-1)!} \\ 0 & 0 & 1 & \cdots & \frac{\lambda^{\rho_i-3}}{(\rho_i-2)!} \\ \vdots & & \ddots & \ddots & \vdots \\ 0 & & \cdots & 0 & 1 \\ 0 & 0 & \cdots & & 0 \end{bmatrix}, \quad \boldsymbol{B}_k^i := \begin{bmatrix} \frac{\lambda^{\rho_i-1}}{\rho_i!} \\ \frac{\lambda^{\rho_i-2}}{(\rho_i-1)!} \\ \vdots \\ \lambda/2 \\ 1 \end{bmatrix} \quad \boldsymbol{C}_k^i := \begin{bmatrix} 1 & 0 & \cdots & 0 \end{bmatrix}, \quad i = 1, \ldots, m.$$

and therefore, the model is explicitly defined in terms of the approximated analytical functions $\boldsymbol{l}(\boldsymbol{\xi}_k,\boldsymbol{\eta}_k)$, $\boldsymbol{M}(\boldsymbol{\xi}_k,\boldsymbol{\eta}_k)$, $\boldsymbol{f}_s(\boldsymbol{\xi}_k,\boldsymbol{\eta}_k)$, and the system sampling time λ, which are based on the original continuous–time nonlinear model. Note that

$$\lim_{\lambda\to 0}\boldsymbol{A}_k^i \to \boldsymbol{A}_o^i, \quad \lim_{\lambda\to 0}\boldsymbol{B}_k^i \to \boldsymbol{B}_o^i \tag{68}$$

which recovers the original continuous time normal form for small sampling times [75]. Furthermore, the local truncation error between the output $\boldsymbol{y}_k = \boldsymbol{C}_c\boldsymbol{\xi}_k$ of the discrete-time nonlinear model and the true system output $\boldsymbol{y}(t)$ is of order $\lambda^{\rho+1}$. This results in a well approximated sampled–data system for sufficiently small sampling times and low relative degrees (1 or 2). Considering the sampled vector $\boldsymbol{\varphi}(\boldsymbol{\xi}_k,\boldsymbol{\eta}_k)$ and sampled matrix $\boldsymbol{\vartheta}(\boldsymbol{\xi}_k,\boldsymbol{\eta}_k)$ as

$$\boldsymbol{\varphi}(\boldsymbol{\xi}_k,\boldsymbol{\eta}_k) = \left[-\boldsymbol{M}(\boldsymbol{\xi}_k,\boldsymbol{\eta}_k)^{-1}\boldsymbol{l}(\boldsymbol{\xi}_k,\boldsymbol{\eta}_k)\right] \tag{69a}$$

$$\boldsymbol{\vartheta}(\boldsymbol{\xi}_k,\boldsymbol{\eta}_k) = \boldsymbol{M}(\boldsymbol{\xi}_k,\boldsymbol{\eta}_k)^{-1} \tag{69b}$$

and denoting $\boldsymbol{\nu}_k$ as the sampled–time virtual control input, the state feedback control law $\boldsymbol{u}_k$ defined as

$$\boldsymbol{u}_k = \boldsymbol{\varphi}(\boldsymbol{\xi}_k,\boldsymbol{\eta}_k) + \boldsymbol{\vartheta}(\boldsymbol{\xi}_k,\boldsymbol{\eta}_k)\boldsymbol{\nu}_k = \boldsymbol{M}(\boldsymbol{\xi}_k,\boldsymbol{\eta}_k)^{-1}\left[\boldsymbol{\nu}_k - \boldsymbol{l}(\boldsymbol{\xi}_k,\boldsymbol{\eta}_k)\right] \tag{70}$$

cancels all nonlinearities in closed-loop in absence of external disturbances and model uncertainties, resulting in the system represented in the following approximated discrete normal form

$$\delta\boldsymbol{\xi}_k = \boldsymbol{A}_s\boldsymbol{\xi}_k + \boldsymbol{B}_s\boldsymbol{\nu}_k \tag{71a}$$

$$\delta\boldsymbol{\eta}_k = \boldsymbol{f}_s(\boldsymbol{\xi}_k,\boldsymbol{\eta}_k) \tag{71b}$$

$$\boldsymbol{y}_k = \boldsymbol{C}_c\boldsymbol{\xi}_k \tag{71c}$$

which is still described in normal form and decomposed into an external (input–output) part and an internal (unobservable) part. In this case, this sampled–data model is driven by the sampled–time virtual control input and approximated by the corresponding sampled z_k–coordinates $(\boldsymbol{\eta}_k, \boldsymbol{\xi}_k)$. The sampled–data model (67) results in having a vector of relative degree $\boldsymbol{\rho}_k = [\,\rho_{k_1} \quad \ldots \quad \rho_{k_p}\,]^\top = [\,1 \quad \ldots \quad 1\,]^\top$ with respect to the output $\boldsymbol{y}_k$ [64, 65] and furthermore, the discrete-time zero dynamics are given by two subsystems, namely the sampled counterpart of the continuous–time zero dynamics $\delta\boldsymbol{\eta}_k = \boldsymbol{f}_s(\boldsymbol{0},\boldsymbol{\eta}_k)$ and a linear subsystem of dimension denoted as $\bar{\boldsymbol{\rho}} = [\,\rho_1 - 1 \quad \ldots \quad \rho_p - 1\,]^\top$. From the approximated model (67) it is clear that we can collect the ρ shifted outputs with a slight abuse of notation as

$$\delta\boldsymbol{z}_{(\boldsymbol{\rho})(k)} = \boldsymbol{l}(\boldsymbol{\eta}_k,\boldsymbol{\xi}_k) + \boldsymbol{M}(\boldsymbol{\eta}_k,\boldsymbol{\xi}_k)\boldsymbol{u}_k = \boldsymbol{\nu}_k \tag{72a}$$

and note that the relationship between the continuous–time $\boldsymbol{\rho}$ differentiated outputs and the shifted state variables is given by the forward Euler method also obtained by a truncated Taylor series expansion, i.e., as

$$\boldsymbol{y}^{(\rho)} \cong \delta\boldsymbol{z}_{(\boldsymbol{\rho})(k)} = \frac{\boldsymbol{z}_{(\boldsymbol{\rho})(k+1)} - \boldsymbol{z}_{(\boldsymbol{\rho})(k)}}{\lambda} \tag{73}$$

where again, a linear input–output relationship between the $\boldsymbol{\nu}_k$ and the output $\boldsymbol{y}_k$ is precluded by the condition of $\boldsymbol{M}(\boldsymbol{\eta}_k,\boldsymbol{\xi}_k)^{-1}$ being nonsingular.

C. Incremental Nonlinear Dynamic Inversion in Sampled–Data Form

We are now interested in the main result of this paper, which is a sampled–data form of the incremental nonlinear dynamic inversion control so far considered. Notice that, generally speaking, the nonlinear control laws uses the approximated or estimated model described by $\bar{\boldsymbol{M}}$ and $\bar{\boldsymbol{l}}$ as

$$\boldsymbol{u}_k = \bar{\boldsymbol{M}}(\boldsymbol{\eta}_k, \boldsymbol{\xi}_k)^{-1} \left[\boldsymbol{\nu}_k - \bar{\boldsymbol{l}}(\boldsymbol{\eta}_k, \boldsymbol{\xi}_k)\right] \tag{74}$$

which causes a problem in terms of uncertainties since inserting this control law gives

$$\delta\boldsymbol{\xi}_k = \boldsymbol{A}_s\boldsymbol{\xi}_k + \boldsymbol{B}_s \left\{\boldsymbol{l}(\boldsymbol{\eta}_k, \boldsymbol{\xi}_k) + \boldsymbol{M}(\boldsymbol{\eta}_k, \boldsymbol{\xi}_k)\bar{\boldsymbol{M}}(\boldsymbol{\eta}_k, \boldsymbol{\xi}_k)^{-1} \left[\boldsymbol{\nu}_k - \bar{\boldsymbol{l}}(\boldsymbol{\eta}_k, \boldsymbol{\xi}_k)\right]\right\} \tag{75}$$

resulting in the closed–loop dynamics

$$\delta\boldsymbol{\xi}_k = (\boldsymbol{A}_s - \boldsymbol{K}\boldsymbol{B}_s)\,\boldsymbol{\xi}_k + \boldsymbol{\epsilon}_{NDI} \tag{76}$$

which is not linearizing anymore because of the extra term $\boldsymbol{\epsilon}_{NDI}$ containing uncertain nonlinear terms [57, 58]. This major flaw of NDI–based control systems is well known, and also previously demonstrated by [34, 76, 77]. In order to partially tackle this flaw of NDI, we are now interested in obtaining an INDI control but in a sampled–data framework. To design a sampled–data form incremental nonlinear dynamic inversion, first we introduce the following assumption.

Small time delay (STD) assumption: *For a sufficiently small time-delay λ so that $\boldsymbol{l}(\boldsymbol{\eta}_k, \boldsymbol{\xi}_k)$ and $\boldsymbol{M}(\boldsymbol{\eta}_k, \boldsymbol{\xi}_k)$ does not vary significantly during λ, we assume the following approximations to hold*:

$$\epsilon_{STD_l}(t) \equiv \boldsymbol{l}(\boldsymbol{\eta}_k, \boldsymbol{\xi}_k) - \boldsymbol{l}(\boldsymbol{\eta}_{k-1}, \boldsymbol{\xi}_{k-1}) \cong \boldsymbol{0} \tag{77}$$

$$\epsilon_{STD_M}(t) \equiv \boldsymbol{M}(\boldsymbol{\eta}_k, \boldsymbol{\xi}_k) - \boldsymbol{M}(\boldsymbol{\eta}_{k-1}, \boldsymbol{\xi}_{k-1}) \cong \boldsymbol{0} \tag{78}$$

this implies that

$$\boldsymbol{l}(\boldsymbol{\eta}_k, \boldsymbol{\xi}_k) \cong \boldsymbol{l}(\boldsymbol{\eta}_{k-1}, \boldsymbol{\xi}_{k-1}) = \delta\boldsymbol{z}_{(\boldsymbol{\rho})(k-1)} - \boldsymbol{M}(\boldsymbol{\eta}_{k-1}, \boldsymbol{\xi}_{k-1})\boldsymbol{u}_{k-1} \tag{79}$$

which, by defining the following deviation variables

$$\Delta\delta\boldsymbol{z}_{(\boldsymbol{\rho})(k)} := \delta\boldsymbol{z}_{(\boldsymbol{\rho})(k)} - \delta\boldsymbol{z}_{(\boldsymbol{\rho})(k-1)}, \tag{80a}$$

$$\Delta\boldsymbol{u}_k := \boldsymbol{u}_k - \boldsymbol{u}_{k-1}, \tag{80b}$$

and in virtue of (78) *(as in the TSS assumption),* (79) *leads to*

$$\Delta\delta\boldsymbol{z}_{(\boldsymbol{\rho})(k)} \cong \boldsymbol{M}(\boldsymbol{\eta}_{k-1}, \boldsymbol{\xi}_{k-1})\Delta\boldsymbol{u}_k \tag{81}$$

in other words

$$\delta\boldsymbol{z}_{(\boldsymbol{\rho})(k)} \cong \delta\boldsymbol{z}_{(\boldsymbol{\rho})(k-1)} + \boldsymbol{M}(\boldsymbol{\eta}_{k-1}, \boldsymbol{\xi}_{k-1})\,(\boldsymbol{u}_k - \boldsymbol{u}_{k-1}) + \mathcal{O}(\lambda^{\rho+1}). \tag{82}$$

Recalling the control law in Eq. (74), and considering our given STD assumption, we may now use

$$\bar{\boldsymbol{l}}(\boldsymbol{\eta}_k, \boldsymbol{\xi}_k) = \boldsymbol{l}(\boldsymbol{\eta}_{k-1}, \boldsymbol{\xi}_{k-1}) \tag{83}$$

which is given by Eq. (79) and by applying nonlinear dynamic inversion results into the following sampled–time INDI controller

$$\boldsymbol{u}_k = \boldsymbol{u}_{k-1} + \bar{\boldsymbol{M}}(\boldsymbol{\eta}_k, \boldsymbol{\xi}_k)^{-1} \left[\boldsymbol{\nu}_k - \delta\boldsymbol{z}_{(\boldsymbol{\rho})(k-1)}\right] \tag{84}$$

where

$$\bar{\boldsymbol{M}}(\boldsymbol{\eta}_k, \boldsymbol{\xi}_k) := \boldsymbol{M}(\boldsymbol{\eta}_{k-1}, \boldsymbol{\xi}_{k-1}) \tag{85}$$

and

$$\delta\boldsymbol{z}_{(\boldsymbol{\rho})(k-1)} = \frac{\boldsymbol{z}_{(\boldsymbol{\rho})(k-1)} - \boldsymbol{z}_{(\boldsymbol{\rho})(k-2)}}{\lambda} \tag{86}$$

Referring back to the attitude control problem, since we will depart from the (approximated) **discrete normal form** in (71) for the control design, the application of *INDI* results in a control law that is also depending only on the uncertainties contained within the ICE matrix

$$\boldsymbol{u}_k = \boldsymbol{u}_{k-1} + \boldsymbol{M}(\boldsymbol{\eta}_{k-1}, \boldsymbol{\xi}_{k-1})^{-1} \left[\boldsymbol{\nu}_k - \delta\boldsymbol{z}_{(\boldsymbol{\rho})(k-1)}\right] \tag{87}$$

However, notice that

$$\boldsymbol{M}(\boldsymbol{\eta}_{k-1}, \boldsymbol{\xi}_{k-1}) = \underbrace{\nabla[\mathcal{L}_f^1 \boldsymbol{h}(\boldsymbol{x}_{k-1})]}_{\text{purely kinematic}} \quad \underbrace{\bar{\boldsymbol{G}}}_{\text{purely parametric}} \tag{88}$$

The purely kinematic term in the resulting control law is only subjected to the measured errors contained in $\boldsymbol{x}_{k-1}$. For the sampled–time attitude control, we have the following sampled quantities

$$\boldsymbol{\xi}_k = \boldsymbol{\psi}_s(\boldsymbol{x}_k) = \begin{bmatrix} z_{k_1} \\ z_{k_2} \\ z_{k_3} \\ z_{k_4} \\ z_{k_5} \\ z_{k_6} \end{bmatrix} = \begin{bmatrix} \sigma_{k_1} \\ \dot{\sigma}_{k_1} \\ \sigma_{k_2} \\ \dot{\sigma}_{k_2} \\ \sigma_{k_3} \\ \dot{\sigma}_{k_3} \end{bmatrix} \tag{89}$$

and notice that the system has a vector of relative degree $\boldsymbol{\rho}_k = [\, \rho_{k_1} \quad \rho_{k_2} \quad \rho_{k_3} \,]^\top = [\, 1 \quad 1 \quad 1 \,]^\top$ with respect to the output $\boldsymbol{y}_k$. To conclude the *INDI* attitude control design, we have made use of the fact that, because of (86), we can rewrite

$$\delta\dot{\boldsymbol{\sigma}}_k = \frac{\dot{\boldsymbol{\sigma}}_k - \dot{\boldsymbol{\sigma}}_{k-1}}{\lambda} \cong \ddot{\boldsymbol{\sigma}}_k \tag{90}$$

and therefore

$$\delta z_{(\boldsymbol{\rho})(k-1)} = \ddot{\boldsymbol{\sigma}}_{k-1} = \frac{1}{4} \left[\, \dot{\boldsymbol{B}}(\boldsymbol{\sigma}_{k-1}) \cdot \boldsymbol{\omega}_{k-1} + \boldsymbol{B}(\boldsymbol{\sigma}_{k-1}) \cdot \dot{\boldsymbol{\omega}}_{k-1} \,\right] \tag{91}$$

where the relationship

$$\begin{aligned} \dot{\boldsymbol{B}}(\boldsymbol{\sigma}_{k-1}) \cdot \boldsymbol{\omega}_{k-1} = \frac{1}{2} \Big[\, & 2\boldsymbol{\sigma}_{k-1}^T \boldsymbol{\omega}_{k-1} (1 - \boldsymbol{\sigma}_{k-1}^T \boldsymbol{\sigma}_{k-1}) \boldsymbol{\omega}_{k-1} \\ & -(1 + \boldsymbol{\sigma}_{k-1}^T \boldsymbol{\sigma}_{k-1}) \boldsymbol{\omega}_{k-1}^T \boldsymbol{\omega}_{k-1} \boldsymbol{\sigma}_{k-1} - 4\boldsymbol{\sigma}_{k-1}^T \boldsymbol{\omega}_{k-1} \boldsymbol{S}\left(\boldsymbol{\omega}_{k-1}\right) \boldsymbol{\sigma}_{k-1} + 4(\boldsymbol{\sigma}_{k-1}^T \boldsymbol{\omega}_{k-1})^2 \boldsymbol{\sigma}_{k-1} \,\Big] \end{aligned} \tag{92}$$

is given analytically. By virtue of eigenvalue assignment, we may find $\boldsymbol{\nu}_k$ such that

$$\boldsymbol{\nu}_k = -\boldsymbol{K}\boldsymbol{\psi}(\boldsymbol{x}_k) = -\boldsymbol{K}\boldsymbol{\xi}_k \tag{93}$$

obtaining therefore the following closed-loop system in absence of model uncertainties and perturbations

$$\delta\boldsymbol{\xi}_k = (\boldsymbol{A}_s - \boldsymbol{B}_s \boldsymbol{K})\, \boldsymbol{\xi}_k \tag{94a}$$

$$\delta\boldsymbol{\eta}_k = \boldsymbol{f}_s(\boldsymbol{\eta}_k, \boldsymbol{\xi}_k) \tag{94b}$$

$$\boldsymbol{y}_{k,CL} = \boldsymbol{C}_s \boldsymbol{\xi}_k \tag{94c}$$

where again, the local truncation error between $\boldsymbol{y}_{k,CL}$ and $\boldsymbol{y}(t)$ is of order $[\, \lambda^{\rho_1+1} \quad \ldots \quad \lambda^{\rho_P+1} \,]^\top$. This concludes the control design using the sampled–data form of incremental nonlinear dynamic inversion for spacecraft attitude control.

V. Attitude Control Simulations

For numerical simulations using the comprehensive analytical nonlinear model of Sec. II, we consider the satellite platform BIROS (*Bispectral InfraRed Optical System*) [3] which was successfully launched into space on 22nd June 2016 at 05:55 CEST, and is the second technology demonstrator along with the TET-1 satellite of the DLR R&D 'FireBIRD'[4] space mission aiming to provide infrared (IR) remote sensing for early fire detection (forest fires, volcanic activity, gas flares and industrial hotspots). These small satellites are extensions and largely based on the flight-proven BIRD (*Bi-spectral Infra-Red Detection*) satellite bus launched in 2001 [78, 79]. Among several mission goals and scientific experiments, to demonstrate a high-agility attitude control system, the platform is actuated with an array of three orthogonal *'High-Torque-Wheels'* (HTW) [1, 2]. The *HTWs* are placed in an orthogonal configuration, which

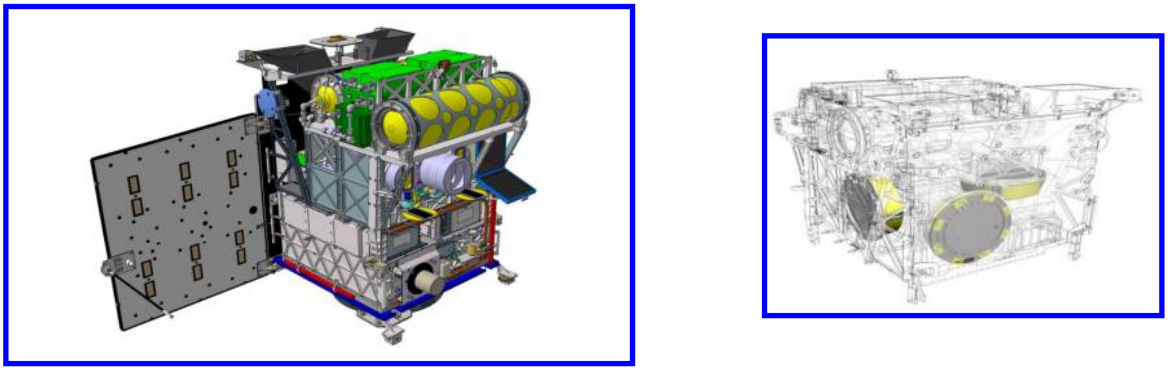

(a) BIROS CAD drawing

(b) *'High-Torque-Wheels'* (yellow) at BIROS payload compartment

Fig. 1 BIROS (*Bispectral InfraRed Optical System*) satellite and its array of three *'High-Torque-Wheels'*. Image credits [3], DLR.

means that the satellite's reaction wheel array alignment matrix is simply $\boldsymbol{A} = \text{diag}([\,1 \quad 1 \quad 1\,])$. Wheel characteristics for these *HTW*s are presented in Table 1.

For agile reorientation, however, a challenge arises from the fact that fast slew maneuvers are in general not of the *Euler-axis* rotation type [11, 12], specially whenever the actuators are constrained independently [13] as it will be in our case. Moreover, BIROS' On-Board-Computer (OBC) can only accomodate rotational acceleration or torque commands up to twice per second (2 Hz) which means that these commands must be piece–wise constant sampled–time control inputs. In [10], the problem of designing fast slew maneuvers was considered as a trajectory optimization problem. However, these optimized slews are hardly implementable in practice, even less when agility is required *on demand*. Generally speaking, on–board trajectory optimization is very computationally demanding and can consume considerable time to obtain feasible solutions. For those reasons, we are interested in performing on–board agile maneuvers by means of our sampled–data formulation of INDI in combination with a simple path planner which can command large angle maneuvers to be tracked by the closed–loop control system. In the simulations to be performed, we consider BIROS to have an inertia matrix of

$$\boldsymbol{I} = \begin{bmatrix} 10 & 1 & 0.5 \\ 1 & 7 & 0.2 \\ 0.5 & 0.2 & 9 \end{bmatrix} \text{Kg} \cdot \text{m}^2$$

The initial *HTW* wheel speeds are set to zero since we will consider these wheels only for agile reorientation; normally

Table 1 Wheel characteristics

Performance	*HTW*
Max. speed [rad/s]	300
Nominal torque [Nm]	0.21
Max. torque [Nm]	0.25
Mechanics	
Moment of inertia [$\text{Kg} \cdot \text{m}^2$]	5×10^{-3}

during operation, wheel speeds have some initial conditions that represents the angular momentum stored in the satellite platform. The nominal operation values presented in Table 1 are considered as the actuator limits in order to restrict

the demands of the attitude maneuver as to avoid the case when wheels must be saturated by their respective control commands.

Because the focus of this paper is to introduce a sampled–data formulation for INDI controllers, we shall focus first on the numerical analysis without actuator and sensor dynamics in order to test this formulation in practice. It is well known from the literature [50, 51, 57, 80] that the actuator dynamics have to be "sufficiently" fast and also synchronized with the sensor and the filters in order to avoid undesired interaction between the controller and the plant due to the time–delayed sensor measurements, estimates, and incremental control actions. Not having synchronized signals between the time–delayed sensor signal and the time–delayed actuator signal might cause instability issues in INDI [50, 81]. In that sense, and actually corroborated in practice, the reaction–wheel "inner–loop" which is commanded by a desired torque provides the output at much higher rates from the ones to be simulated (100 Hz) and therefore, we neglect these actuator dynamics.

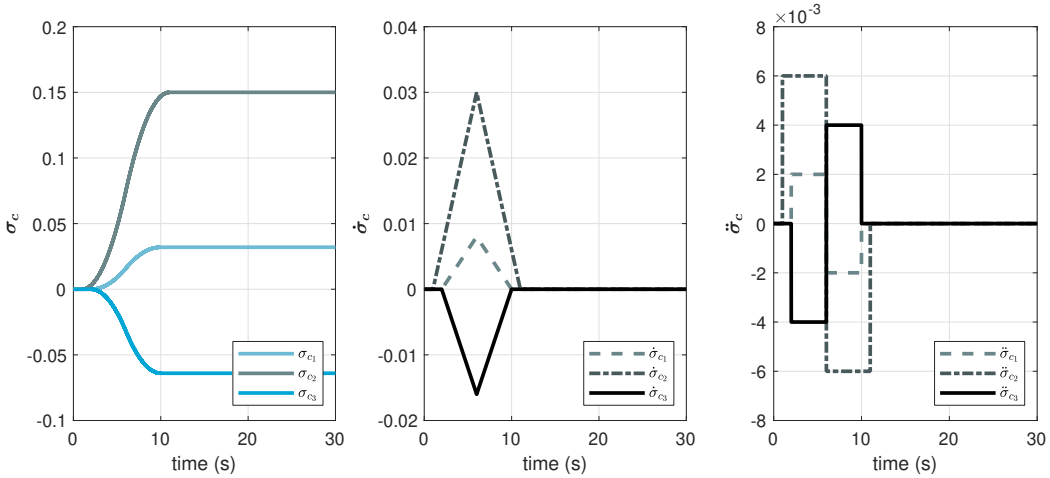

Fig. 2 MRP reference tracking commands

The MRP tracking reference commands, illustrated in Fig. 2, are designed to be smoothly up to a second order and obtained with a simple reference trajectory generator. The feedforward acceleration command is designed as a piece–wise "doublet" discrete signal. This acceleration profile can be integrated twice in discrete–time to obtain the corresponding MRP and MRP rate commands that are going to be used as the reference. This approach for reference command generation (that can be seen as a motion/trajectory/path planner) is quite important because the resulting feedforward acceleration will produce a moment command that corresponds closely to the path specified, hence why we can approximate the MRP attitude error by the algebraic expression presented (MRP additive error) and not using the MRP multiplicative error (by composition or relative orientations). The rest-to-rest maneuver is designed to achieve a desired final attitude by performing full three–axis control without an optimizer to design the resulting profile. It is important to mention that this trajectory is a time–dependent attitude path for the MRP specified a-priori, giving the satellite's on board computer the capability to perform agile maneuvers on demand without having to request an optimization routine to find a time optimal path dynamically. For all simulations we consider the virtual controller $\boldsymbol{\nu} = \ddot{\mathbf{y}}_d + \mathbf{k}_D\dot{\boldsymbol{e}} + \mathbf{k}_P\boldsymbol{e}$ so that the (second order) error dynamics

$$\ddot{\boldsymbol{e}} + \mathbf{k}_D\dot{\boldsymbol{e}} + \mathbf{k}_P\boldsymbol{e} = \mathbf{0} \tag{95}$$

are equivalent across the different scenarios considered. This is a classical second order dynamics where considering a natural frequency ω_n and damping coefficient of ζ we can obtain the gains

$$\mathbf{k}_{D_i} = 2 \cdot \zeta \cdot \omega_n, \; i = 1, 2, 3 \tag{96a}$$

$$\mathbf{k}_{P_i} = \omega_n^2, \; i = 1, 2, 3 \tag{96b}$$

For all simulations we fix $\zeta = 0.707$ and leave ω_n as a tuning parameter depending on the sampling of the controller.

The simulation results are as follows. This first simulation is done at a sampling of 10 Hz which is already quite close to simulation results using a sampling of 100 Hz (not shown). In this case, we set $\omega_n = 1$ rad/s. For the attitude

control motion obtained, see Fig. 3; it can be seen that the MRP attitude tracking profile is quite satisfactory because of the tracking errors shown. Along with these results, Fig. 4 shows the resulting angular velocity of the spacecraft together with the angular velocity of the reaction wheels while Fig. 5 shows the corresponding *HTW* virtual control input together with the resulting commanded wheel torques (input control) using the sampled–data INDI control. This maneuver showcases also that the limits have been avoided and that the platform is commanded with high-agility.

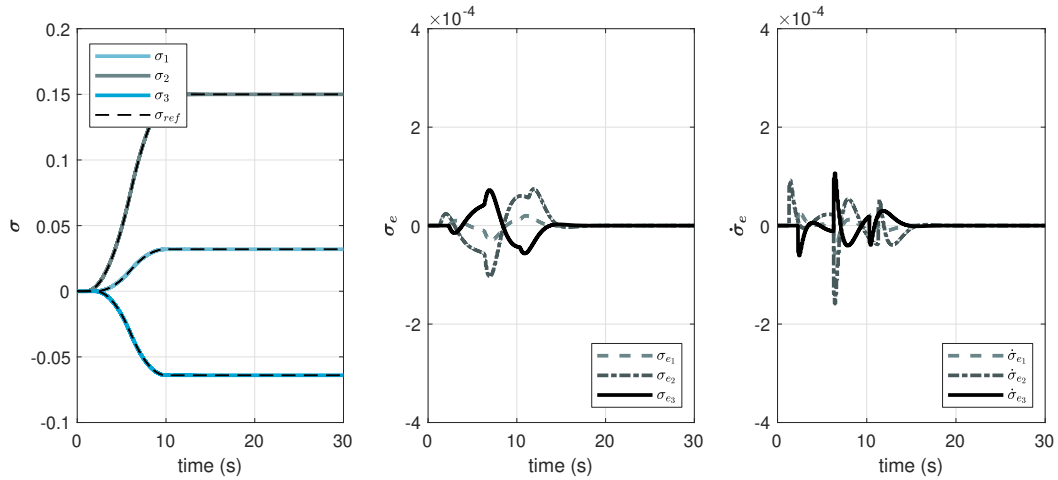

Fig. 3 INDI control at 10 Hz: MRP attitude tracking profile (left) and its corresponding tracking errors, σ_e (middle) and $\dot{\sigma}_e$ (right).

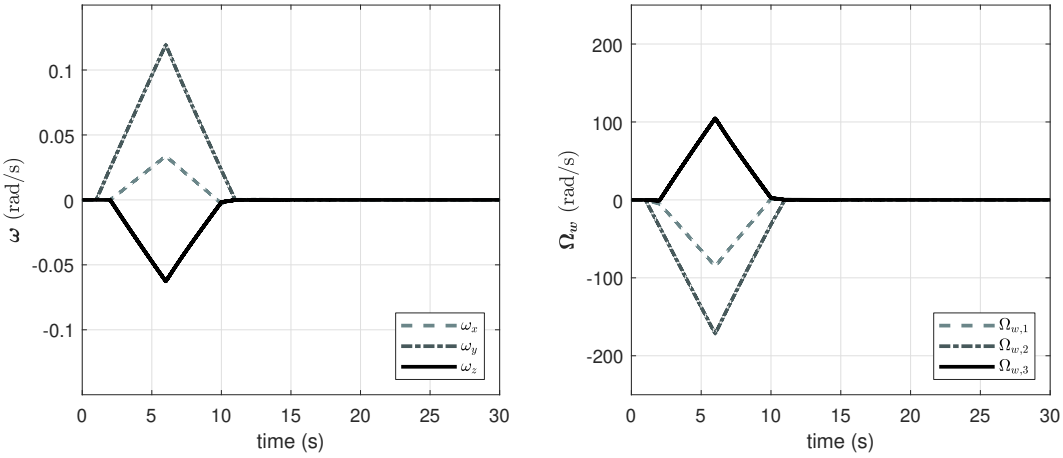

Fig. 4 INDI control at 10 Hz: resulting angular velocity of the spacecraft (left) and angular velocity of the reaction wheels (right).

A second simulation is performed where the sampling time has been set to 1 Hz. In this case, we set $\omega_n = 0.1$ rad/s because this parameter has a strong influence on the tracking performance as well as on the stability of the closed–loop control system which is operating on a such low sampling rate. During simulations it was found that this relationship or dependency can be further analyzed to improve the response of the system, but this falls out of the scope of this paper. Moreover, for this simulation we have perturbed the plant by adding inertia parametric uncertainties to also test the robustness of our sampled–data INDI controller. Table 2 shows the considered perturbations on the diagonal elements of the inertia matrix, giving rise to 27 combinations that are tested in a (small) Monte Carlo campaign. Figure 6 shows the attitude control motion obtained under these parametric uncertainties together with the resulting tracking errors. Despite the relative big errors obtained, the system demonstrates still being to remain closed-loop stable and performant

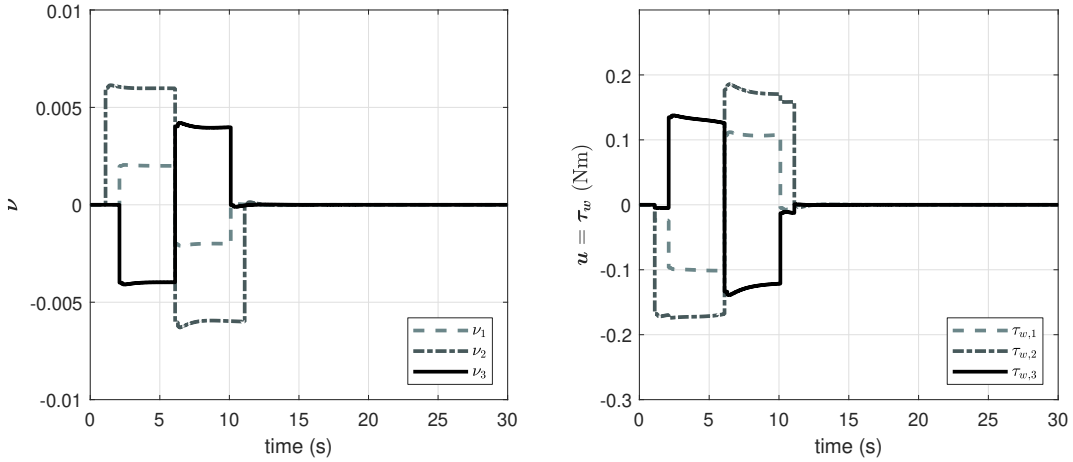

Fig. 5 INDI control at 10 Hz: virtual control ν (left) and commanded wheel torques (right) during the fast slew maneuver.

by completing the desired maneuver under the parametric perturbations considered. In this case, simulation results also demonstrated that the platform can be commanded with high-agility while showcasing that the robustness of this INDI approach is preserved even at a such low sampling rate of 1 Hz. Along with these tracking performance results, Fig. 4 shows the resulting angular velocity of the spacecraft together with the angular velocity of the reaction wheels for all the perturbed cases considered. In these plots it can be seen the piece–wise linear behaviour of these variables since the low–sampling frequency of the control system is more noticeable. This is more evident by inspecting Fig. 5 which shows the corresponding *HTW* virtual control input together with the resulting commanded wheel torques (input control) using our sampled–data INDI control. Here, the piece–wise constant nature of these control commands are more evident and clearly shows that INDI control at such low sampling rate of 1 Hz is still possible. However, this maneuver showcases that the platform is operating at the limits of the reaction wheels which calls for a re-assement of the maneuver profile (increase the maneuver time, for instance) or re–tuning of the controller parameter ω_n. This last approach might render the system unstable or not be able to perform as desired; but it is noticeable that changing the motion profile for a less aggressive maneuver, or by allowing more time to complete it, could improve the closed–loop response without much effort on control re-design or control parameter tuning. It is therefore proven that 'down–scaling' the sampling time is feasible with our approach. Of course, there will be a limit on how low can the sampling time be.

In summary, simulation results shows that an agile attitude control system using INDI is promising because of the capability to track agile maneuvers effectively. Having used a sampled–data approach also allows to consider the sampling–time explicitly in the formulations and also to study what happens while decreasing the achievable sampling time of the control computer. In [74, 82] it was shown a relationship between INDI and TDC/PID control where the influences of the parametric uncertainty on the robust performance and stability have been shown to be superior for INDI in comparison to TDC/PID control. This clearly suggests, that although they may have similar performance, the INDI control laws possess better robustness and stability properties. The systematic gain tuning (using the desired error dynamics as a guide) and self scheduling property of our INDI controller (because of the obtained model–based terms) have been shown to be scaled and readily applied to attitude control of rigid spacecraft for agile maneuvers.

Table 2 Uncertainties

Parameter	Nominal Value [Kg · m^2]	Uncertainty
$\boldsymbol{I}_{x,x}$	10	±5 %
$\boldsymbol{I}_{y,y}$	7	±5 %
$\boldsymbol{I}_{z,z}$	9	±5 %

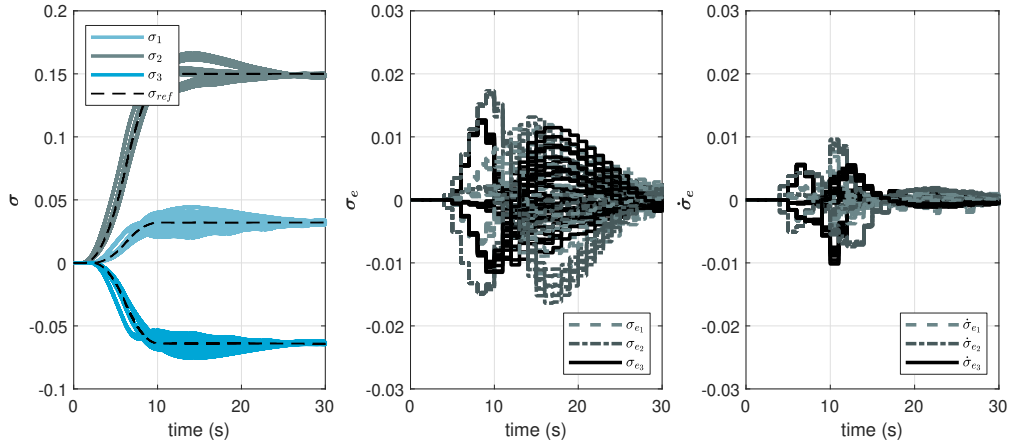

Fig. 6 INDI control at 1 Hz: MRP attitude tracking profile (left) and its corresponding tracking errors, σ_e (middle) and $\dot{\sigma}_e$ (right).

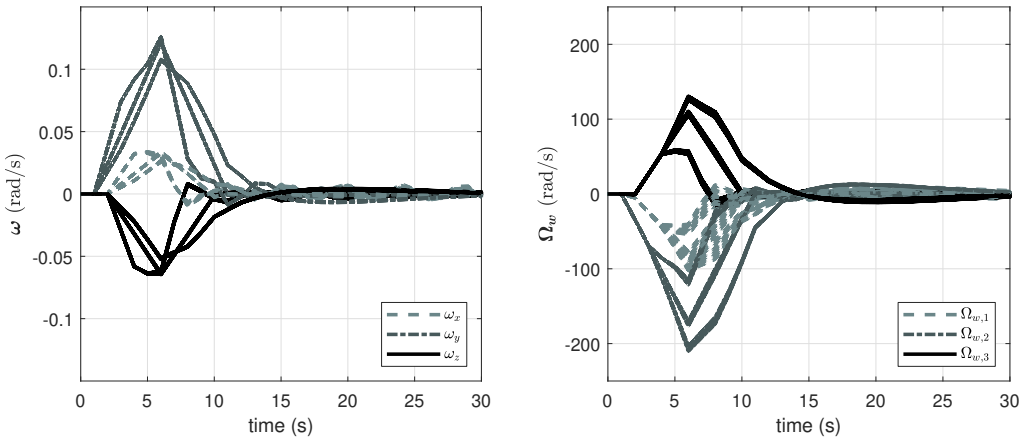

Fig. 7 INDI control at 1 Hz: resulting angular velocity of the spacecraft (left) and angular velocity of the reaction wheels (right).

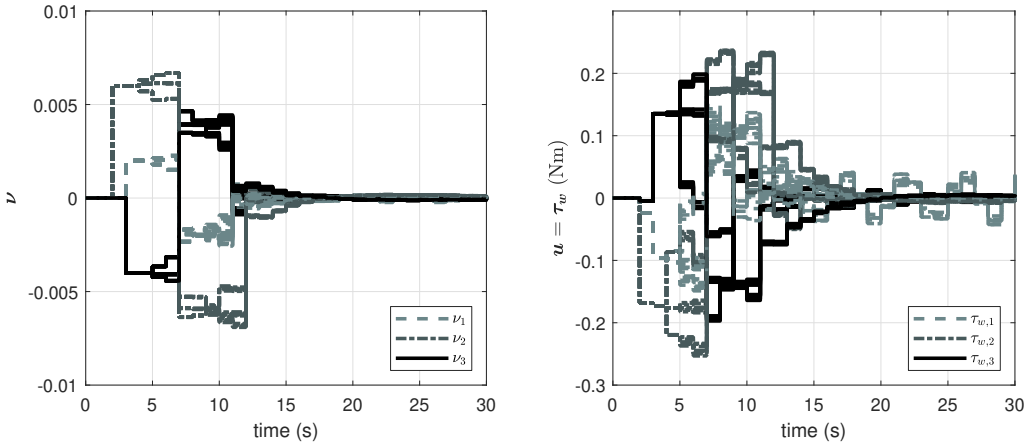

Fig. 8 INDI control at 1 Hz: virtual control ν (left) and commanded wheel torques (right) during the fast slew maneuver.

VI. Conclusion

In this paper a sampled–data form of the recently reformulated incremental nonlinear dynamic inversion (INDI) is proposed and applied in the context of spacecraft attitude control. The objective was to bridge the gap between highly sampled INDI formulations (100 – 1000 Hz) and their lowly sampled counterparts in the context of spacecraft attitude control where low sampling rates are common (1 – 10 Hz) . This was done by introducing a sampled–data reformulation of INDI that allows explicit consideration of the sampling time via an approximate sampled–data model in normal form available in the literature. Having an explicit consideration of the sampling time in the plant and in the controller is important because there is a limit where the stability and performance of the resulting closed–loop nonlinear system can be compromised. Moreover, this sampled–data model is better suited for the INDI controller since it can be applied for plants with higher relative degree than one. Regarding the attitude control, it was done in terms of *Modified Rodrigues Parameters* (MRPs) where the scheduling of the time–varying control effectiveness is achieved with the Jacobian of the MRP kinematics. This is an improvement over similar control strategies previously developed for rigid body spacecraft since it results in an architecture without a cascaded inner–loop based on a time–scale separation assumption for the rate loop which is commonly done. This results in the control effectiveness of the control loop composed entirely of kinematic (fully known) and parametric terms, making it useful as a scheduling term for the robust nonlinear controller. This resulting non–cascaded inversion–based architecture only requires an accurate control effectiveness model and measurements of the state and some of its derivatives resulting in a *combined* model– and sensor–based control approach. Simulations experiments for different sampling times showed the effectiveness of this method.

Acknowledgments

We would like to acknowledge useful discussions and revisions to this manuscript by Tobias Posielek (DLR-SR).

References

[1] Raschke, C., Terzibaschian, T., and Halle, W., "High Agility Demonstration with a New Actuator System by Small Satellite BIROS," *"Proc. of the 9th Airtec, Frankfurt/Main"*, 2014.

[2] Raschke, C., Terzibaschian, T., and Halle, W., "A New Actuator System for High Agility Demonstration with the Small Satellite BIROS," *"Proc. of the 10th IAA Symposium on Small Satellites for Earth Observation, Berlin"*, 2015.

[3] Halle, W., Terzibaschian, T., and Rockwitz, K.-D., ""The DLR-BIROS-Satellite for Fire-Detection and Technological Experiments"," *"Proc. of the 10th IAA Symposium on Small Satellites for Earth Observation, Berlin"*, 2015.

[4] Halle, W., Terzibaschian, T., Bärwald, W., and Schultz, C., "The DLR Small-Satellite Constellation FireBIRD," *"Proc. of the 31st International Symposium on Space Technology and Science (ISTS), Matsuyama-Ehime"*, 2017.

[5] Wang, Xinwei and Han, Chao and Zhang, Rui, "Multiple agile Earth observation satellites, oversubscribed targets scheduling using complex networks theory," *arXiv e-prints*, 2018, arXiv:1805.05053.

[6] Han, C., Wang, X., Song, G., and Leus, R., "Scheduling multiple agile Earth observation satellites with multiple observations," *arXiv e-prints*, 2018, arXiv:1812.00203.

[7] Aldinger J. and Lohr J., "Planning for Agile Earth Observation Satellites," *Albert-Ludwigs-Universitat Freiburg, Institut fur Informatik*, 2013.

[8] Beaumet G., Verfaillie G., and Charmeau M., "Autonomous Planning for an Agile Earth-Observing Satellite," *Albert-Ludwigs-Universitat Freiburg, Institut fur Informatik*, 2007.

[9] Zang Yuan, Yingwu Chen, and Renjie He, "Agile Earth Observing Satellites Mission Planning Using Genetic Algorithm Based on High Quality Initial Solutions," *IEEE Congress on Evolutionary Computation, CEC 2014, Beijing, China*, 2014. https://doi.org/10.1109/CEC.2014.6900502.

[10] Acquatella B., P., "Fast slew maneuvers for the High-Torque-Wheels BIROS satellite," *In: Transactions of the Japan Society of Aeronautical and Space Sciences*, Vol. 61, No. 2, 2018, pp. 79–86. https://doi.org/DOI:10.2322/tjsass.61.79.

[11] Bilimoria, K. D., and Wie, B., "Time-optimal Reorientation of a Rigid Axisymmetric Spacecraft," *"Proc. of the AIAA Guidance, Navigation, and Control Conference, New Orleans, LA"*, 1991.

[12] Bilimoria, K. D., and Wie, B., "Time-optimal Three-axis Reorientation of a Rigid Spacecraft," *Journal of Guidance, Control and Dynamics*, Vol. 16, No. 3, 1993, pp. 446–452.

[13] Bai, X., and Junkins, J. L., "New Results for Time-optimal Three-axis Reorientation of a Rigid Spacecraft," *Journal of Guidance, Control and Dynamics*, Vol. 32, No. 4, 2009, pp. 1071–1076.

[14] Junkins, J. L., and Turner, J. D., *Optimal Spacecraft Rotational Maneuvers*, Elsevier Publishing, New York, 1986.

[15] Li, F., and Bainum, P. M., "Numerical Approach for Solving Rigid Spacecraft Minimum Time Attitude Maneuvers," *Journal of Guidance, Control and Dynamics*, Vol. 13, No. 1, 1990, pp. 38–45.

[16] Byers, R. M., and Vadali, S. R., "Quasi-closed-form Solution to the Time-optimal Rigid Spacecraft Reorientation Problem," *Journal of Guidance, Control and Dynamics*, Vol. 16, No. 3, 1993, pp. 453–461.

[17] Ross, I. M., Sekhavat, P., Fleming, A., and Gong, Q., "Optimal Feedback Control: Foundations, Examples, and Experimental Results for a New Approach," *Journal of Guidance, Control and Dynamics*, Vol. 31, No. 2, 2008, pp. 307–321.

[18] Fleming, A., Sekhavat, P., and Ross, I. M., "Minimum-time Reorientation of a Rigid Body," *Journal of Guidance, Control and Dynamics*, Vol. 33, No. 1, 2010, pp. 160–170.

[19] Zhou, H., Wang, D., Wu, B., and Poh, E. K., "Time-optimal Reorientation for Rigid Satellite with Reaction Wheels," *Intl. J. of Control*, Vol. 85, No. 10, 2012, pp. 1452–1463.

[20] Karpenko, M., Bhatt, S., Bedrossian, N., and Ross, I. M., "Flight Implementation of Shortest-time Maneuvers for Imaging Satellites," *Journal of Guidance, Control and Dynamics*, Vol. 37, No. 4, 2014, pp. 1069–1079.

[21] Slotine, J. J., and Li, W., *Applied Nonlinear Control*, Prentice Hall Inc, 1990.

[22] Isidori, A., *Nonlinear Control Systems*, 3rd ed., Springer, 1985.

[23] Nijmeijer, H., and van der Schaft, A., *Nonlinear Dynamical Control Systems*, Springer, 1990.

[24] Krener, A. J., "A Decomposition Theory for Differentiable Systems," *SIAM Journal on Control and Optimization*, Vol. 15, No. 5, 1977, pp. 813–829.

[25] Brockett, R. W., "Feedback Invariants for Nonlinear Systems," *IFAC Congress*, Helsinki, 1978.

[26] Ioannou, P., and Sun, J., *Robust Adaptive Control*, Prentice Hall, Inc, 1996.

[27] Krstić, M., Kanellakopoulos, I., and Kokotović, P., *Nonlinear and Adaptive Control Design*, John Wiley & Sons, 1995.

[28] Kokotović, P. V., and Arcak, M., "Constructive Nonlinear Control: A Historical Perspective," *Automatica*, Vol. 37, No. 5, 2001, pp. 637–662.

[29] Looye, G., "Design of Robust Autopilot Control Laws with Nonlinear Dynamic Inversion," *at–Automatisierungstechnik*, Vol. 49, No. 12, 2001, pp. 523–531.

[30] Looye, G. H., "An Integrated Approach to Aircraft Modelling and Flight Control Law Design," Ph.D. thesis, Delft University of Technology, Faculty of Aerospace Engineering, 2008.

[31] Lombaerts, T. J., Huisman, H. O., Chu, Q. P., Mulder, J. A., and Joosten, D. A., "Flight Control Reconfiguration based on Online Physical Model Identification and Nonlinear Dynamic Inversion," *proceedings of the AIAA Guidance, Navigation, and Control Conference and Exhibit*, American Institute of Aeronautics and Astronautics, Inc. (AIAA-2008-7435)., 2008.

[32] Reiner, J., Balas, G. J., and Garrard, W. L., "Flight Control Design Using Robust Dynamic Inversion and Time-scale Separation," *Automatica*, Vol. 32, No. 11, 1996, pp. 1493–1504.

[33] Smith, P. R., "A Simplified Approach to Nonlinear Dynamic Inversion Based Flight Control," *proceedings of the AIAA Atmospheric Flight Mechanics Conference*, American Institute of Aeronautics and Astronautics, Inc. (AIAA-98-4461), 1998, pp. 762–770.

[34] Sieberling, S., Chu, Q. P., and Mulder, J. A., "Robust Flight Control Using Incremental Nonlinear Dynamic Inversion and Angular Acceleration Prediction," *Journal of Guidance, Control and Dynamics*, Vol. 33, No. 6, 2010, pp. 1732–1742.

[35] Smith, P. R., and Berry, A., "Flight Test Experience of a Nonlinear Dynamic Inversion Control Law on the VAAC Harrier," *Proceedings of the AIAA Atmospheric Flight Mechanics Conference*, American Institute of Aeronautics and Astronautics, Inc. (AIAA-2000-3914), 2000, pp. 132–142.

[36] Bacon, B. J., and Ostroff, A. J., "Reconfigurable Flight Control using Nonlinear Dynamic Inversion with a Special Accelerometer Implementation," *proceedings of the AIAA Guidance, Navigation, and Control Conference and Exhibit*, (AIAA-2000-4565), 2000.

[37] Bacon, B. J., Ostroff, A. J., and Joshi, S. M., "Nonlinear Dynamic Inversion Reconfigurable Controller utilizing a Fault-tolerant Accelerometer Approach," Tech. rep., NASA Langley Research Center, 2000.

[38] Bacon, B. J., Ostroff, A. J., and Joshi, S. M., "Reconfigurable NDI Controller using Inertial Sensor Failure Detection & Isolation," *IEEE Transactions on Aerospace and Electronic Systems*, Vol. 37, No. 4, 2001, pp. 1373–1383.

[39] Looye, G., and Joos, H.-D., ""Design of Autoland Controller Functions with Multi-objective Optimization"," *"Proc. of the AIAA Guidance, Navigation, and Control Conference and Exhibit, Monterey, CA"*, 2002.

[40] Looye, G., and Joos, H.-D., "Design of Autoland Controller Functions with Multiobjective Optimization," *Journal of Guidance, Control and Dynamics*, Vol. 29, No. 2, 2006, pp. 475–484.

[41] Roenneke, A. J., and Well, K. H., "Nonlinear Flight Control for a High-lift Rentry Vehicle," *proceedings of the AIAA Guidance, Navigation, and Control Conference*, 1995.

[42] da Costa, R. R., Chu, Q. P., and Mulder, J. A., "Reentry Flight Controller Design Using Nonlinear Dynamic Inversion," *Journal of Spacecraft and Rockets*, Vol. 40, 2003, pp. 64–71.

[43] Juliana, S., *Re-entry Flight Clearance*, PhD thesis, Delft University of Technology, Faculty of Aerospace Engineering, 2006.

[44] Acquatella B., P., Briese, L. E., and Schnepper, K., "Guidance command generation and nonlinear dynamic inversion control for reusable launch vehicles," *Acta Astronautica*, Vol. 174, 2020, pp. 334–346. https://doi.org/https://doi.org/10.1016/j.actaastro.2020.04.002, URL https://www.sciencedirect.com/science/article/pii/S0094576520301843.

[45] Chen, H. B., and Zhang, S. G., "Robust Dynamic Inversion Flight Control Law Design," *ISSCAA 2008, 2nd International Symposium on Systems and Control in Aerospace and Astronautics*, 2008.

[46] Chu, Q. P., *Spacecraft Attitude Control Systems*, Lecture notes, Delft University of Technology, Faculty of Aerospace Engineering, 2010.

[47] Chu, Q. P., *Advanced Flight Control*, Lecture notes, Delft University of Technology, Faculty of Aerospace Engineering, 2010.

[48] Simplício, P., Pavel, M., van Kampen, E., and Chu, Q. P., "An Acceleration Measurements-based Approach for Helicopter Nonlinear Flight Control using Incremental Nonlinear Dynamic Inversion," *Control Engineering Practice*, Vol. 21, No. 8, 2013, pp. 1065–1077.

[49] Acquatella B., P., Falkena, W., van Kampen, E.-J., and Chu, Q. P., "Robust Nonlinear Spacecraft Attitude Control Using Incremental Nonlinear Dynamic Inversion," *proceedings of the AIAA Guidance, Navigation, and Control Conference*, 2012.

[50] Smeur, E. J., Chu, Q. P., and de Croon, G. C., "Adaptive Incremental Nonlinear Dynamic Inversion for Attitude Control of Micro Air Vehicles," *Journal of Guidance, Control and Dynamics*, Vol. 39, No. 3, 2016, pp. 450–461.

[51] Smeur, E. J., de Croon, G. C., and Chu, Q. P., "Gust Disturbance Alleviation with Incremental Nonlinear Dynamic Inversion," *IEEE/RSJ International Conference on Intelligent Robots and Systems (IROS)*, 2016.

[52] van Ekeren, W., Looye, G., Kuchar, R. O., Chu, Q. P., and van Kampen, E., "Design, Implementation and Flight-Tests of Incremental Nonlinear Flight Control Methods," *Proceedings of the AIAA Guidance, Navigation and Control Conference, AIAA SciTech Forum*, American Institute of Aeronautics and Astronautics, Inc. (AIAA 2018-0384), 2018.

[53] Grondman, F., Looye, G., Kuchar, R. O., Chu, Q. P., and van Kampen, E., "Design and Flight Testing of Incremental Nonlinear Dynamic Inversion-based Control Laws for a Passenger Aircraft," *Proceedings of the AIAA Guidance, Navigation and Control Conference, AIAA SciTech Forum*, American Institute of Aeronautics and Astronautics, Inc. (AIAA 2018-0385), 2018.

[54] Twan Keijzer, Gertjan Looye, Q Ping Chu, and Erik-Jan Van Kampen, "Design and Flight Testing of Incremental Backstepping based Control Laws with Angular Accelerometer Feedback," *Proceedings of the AIAA Scitech 2019 Forum*, American Institute of Aeronautics and Astronautics, Inc. (AIAA 2019-0129), 2019.

[55] Wang, X., van Kampen, E., and Chu, Q.P., "Gust Load Alleviation and Ride Quality Improvement with Incremental Nonlinear Dynamic Inversion," *Proceedings of the AIAA Atmospheric Flight Mechanics Conference, AIAA SciTech Forum*, American Institute of Aeronautics and Astronautics, Inc. (AIAA 2017-0774), 2017.

[56] Wang, X., van Kampen, E., De Breuker, R., and Chu, Q.P., "Flexible Aircraft Gust Load Alleviation with Incremental Nonlinear Dynamic Inversion," *Proceedings of the AIAA Atmospheric Flight Mechanics Conference, AIAA SciTech Forum*, American Institute of Aeronautics and Astronautics, Inc. (AIAA 2018-0774), 2018.

[57] Wang, X., van Kampen, E., Chu, Q.P., and Lu, P., "Stability Analysis for Incremental Nonlinear Dynamic Inversion Control," *Journal of Guidance, Control, and Dynamics*, Vol. 42, No. 5, 2019, pp. 1116–1129.

[58] Wang, X., van Kampen, E., Chu, Q.P., and Lu, P., "Stability Analysis for Incremental Nonlinear Dynamic Inversion Control," *Proceedings of the AIAA Guidance, Navigation and Control Conference, AIAA SciTech Forum*, American Institute of Aeronautics and Astronautics, Inc. (AIAA 2018-1115), 2018.

[59] Wang, X., van Kampen, E., Chu, Q.P., and Lu, P., "Incremental Sliding-Mode Fault-Tolerant Flight Control," *Journal of Guidance, Control, and Dynamics*, Vol. 42, No. 2, 2019, pp. 244–259.

[60] Youcef-Toumi, K., and Ito, O., "A Time Delay Controller for Systems with Unknown Dynamics," *Trans. Of ASME, J. Dyn. Sys., Meas., Contr*, Vol. 112, No. 1, 1990, pp. 133–142.

[61] Je Hyung Jung and Pyung-Hun Chang and Oh-Seok Kwon, "A New Stability Analysis of Time Delay Control for Input/Output Linearizable Plants," *Proceedings of the 2004 American Control Conference. Boston, Massachusetts*, 2004.

[62] Chang, P. H., and Jung, J. H., "A Systematic Method for Gain Selection of Robust PID Control for Nonlinear Plants of Second-Order Controller Canonical Form," *IEEE Transactions on Control Systems Technology*, Vol. 17, No. 2, 2009, pp. 473–483.

[63] Salvatore Monaco and Dorothée Normand-Cyrot, "Advanced Tools for Nonlinear Sampled–Data Systems," *European Journal of Control*, Vol. 13, No. 13, 2007, pp. 221–241.

[64] Juan I. Yuz, "Sampled-Data Models for Linear and Nonlinear Systems," Ph.D. thesis, The University of Newcastle, School of Electrical Engineering and Computer Science, 2005.

[65] Juan I. Yuz and Graham C. Goodwin, "On Sampled-Data Models for Nonlinear Systems," *IEEE Transactions on Automatic Control*, Vol. 50, No. 10, 2005, pp. 1477–1489.

[66] Shuster, M. D., "A Survey of Attitude Representations," *The Journal of the Astronautical Sciences*, Vol. 41, No. 4, 1993, pp. 439–517.

[67] Tsiotras, P., "Stabilization and Optimality Results for the Attitude Control Problem," *Journal of Guidance, Control and Dynamics*, Vol. 19, No. 4, 1996, pp. 772–779.

[68] Hanspeter Schaub, John L. Junkins, *Analytical Mechanics of Space Systems*, 1st ed., American Institute of Aeronautics and Astronautics – Technology & Engineering, 2003.

[69] Bang, L. J., H., and Eun, Y., "Nonlinear attitude control for a rigid spacecraft by feedback linearization," *KSME International Journal*, , No. 18, 2004, pp. 203 – 210. https://doi.org/https://doi.org/10.1007/BF03184729.

[70] Khalil, H. K., *Nonlinear Systems*, 3rd ed., Prentice Hall, 2002.

[71] Jizheng, C., Jianping, Y., and Qun, F., "Flight Vehicle Attitude Determination Using the Modified Rodrigues Parameters," *Chinese Journal of Aeronautics*, Vol. 21, No. 5, 2008, pp. 433 – 440. https://doi.org/https://doi.org/10.1016/S1000-9361(08)60056-4.

[72] Acquatella B., P., van Kampen, E., and Chu, Q. P., "Incremental Backstepping for Robust Nonlinear Flight Control," *EuroGNC 2013, 2nd CEAS Specialist Conference on Guidance, Navigation, and Control*, 2013.

[73] Acquatella B., P., *Robust Nonlinear Spacecraft Attitude Control: an Incremental Backstepping Approach*, MSc thesis, Delft University of Technology, Faculty of Aerospace Engineering, 2011.

[74] Acquatella B., P., and Chu, Q. P., "Agile Spacecraft Attitude Control: an Incremental Nonlinear Dynamic Inversion Approach," *In: IFAC-PapersOnLine*, Vol. 90, No. 1, 2020, pp. 8175–8180.

[75] Juan I. Yuz and Graham C. Goodwin, *Sampled-Data Models for Linear Nonlinear Systems*, 2014.

[76] Juliana, S., Chu, Q. P., Mulder, J. A., and van Baten, T. J., "The Analytical Derivation of Nonlinear Dynamic Inversion Control for Parametric Uncertain Systems," *proceedings of the AIAA Guidance, Navigation, and Control Conference*, 2005.

[77] Juliana, S., Chu, Q. P., Mulder, J. A., and van Baten, T. J., "Flight Control of Atmospheric Re-entry Vehicle with Nonlinear Dynamic Inversion," *proceedings of the AIAA Guidance, Navigation, and Control Conference*, 2006.

[78] Briess, K., Bärwald, W., Gill, E., Kayal, H., Montenbruck, O., Montenegro, S., Halle, W., Skrbek, W., Studemund, H., T., T., and Venus, H., "Technology Demonstration by the BIRD-mission," *Acta Astronautica*, Vol. 56, 2005, pp. 57–63.

[79] Zhukov, B., Briess, K., Lorenz, E., Oertel, D., and Skrbek, W., "Detection and Analysis of High-temperature Events in the BIRD mission," *Acta Astronautica*, Vol. 56, 2005, pp. 65–71.

[80] Y. C. Wang, W. S. Chen, S. X. Zhang, J. W. Zhu, and L. J. Cao, "Command-Filtered Incremental Backstepping Controller for Small Unmanned Aerial Vehicles," *Journal of Guidance, Control and Dynamics*, Vol. 41, No. 4, 2018, pp. 954–967.

[81] Vlaar, C., *Incremental Nonlinear Dynamic Inversion Flight Control*, MSc thesis, Delft University of Technology, Faculty of Aerospace Engineering, 2014.

[82] Acquatella B., P., van Ekeren, W., and Chu, Q. P., "PI(D) tuning for flight control systems via Incremental Nonlinear Dynamic Inversion," *In: IFAC-PapersOnLine*, Vol. 50, No. 1, 2017, pp. 8175–8180.